


Photoelectrochemical Energy Conversion over 2D Materials

Ali Raza ^{1,†}, Xinyu Zhang ^{2,3,†}, Sarfraz Ali ^{4,†}, Changhai Cao ^{5,*}, Arslan Ahmed Rafi ⁴ and Gao Li ^{2,*} 

¹ Department of Physics, University of Sialkot (USKT), Sialkot 51040, Pakistan; ali.raza.physics@uskt.edu.pk

² State Key Laboratory of Catalysis, Dalian Institute of Chemical Physics, Chinese Academy of Sciences, Dalian 116023, China; zhangxy04@yeah.net

³ College of Science, Inner Mongolia Agricultural University, Hohhot 010018, China

⁴ Department of Physics, Riphah Institute of Computing and Applied Sciences (RICAS), Riphah International University, Lahore 54000, Pakistan; raisarfrazali70@gmail.com (S.A.); arslanahmedrafi@gmail.com (A.A.R.)

⁵ Key Laboratory of Biofuels and Biochemical Engineering, SINOPEC Dalian Research Institute of Petroleum and Petro-Chemicals, Dalian 116045, China

* Correspondence: sdlgcch@126.com (C.C.); gaoli@dicp.ac.cn (G.L.)

† These authors contributed equally to this work.

Abstract: The solar motivated photoelectrochemical (PEC), used in water splitting systems, shows superior talent in converting solar energy in the form of cleaning and in sustaining a chemical energy evolution. PEC systems present by integrating a photoelectrode, which involves light-harvesting to absorb solar energy, thereby introducing an interlayer for the transformation of photogenerated electrons and holes, along with a co-catalyst to trigger oxidation and reduce the chemical reactions. In this review, we describe a variety of two-dimensional (2D) layered photoanodes and photocathodes, such as graphitic carbon nitrides, transition metal dichalcogenides, layered double hydroxides, MXenes, and co-catalysts for the assembly of combined photoelectrodes belonging to oxygen evolution and/or hydrogen evolution chemical reactions. The basic principles of PEC water splitting associated with physicochemical possessions relating to photoelectrodes unified with catalytic chemical reactions have been investigated. Additionally, the mechanisms attributing to a relationship with 2D photoelectrodes have been incorporated as a supplementary discussion. The improvement strategies, which include the construction of heterostructures, surface functionalization, and formations of heterojunctions, have also been discussed. The issues and challenges relevant to the field have been acknowledged for facilitating future research, indicating optimized conversion activity corresponding to PEC water splitting.

Keywords: photoelectrochemical; photoelectrodes; hydrogen evolution reaction; oxygen evolution reaction; water splitting; heterostructures; surface functionalization



Citation: Raza, A.; Zhang, X.; Ali, S.; Cao, C.; Rafi, A.A.; Li, G.

Photoelectrochemical Energy

Conversion over 2D Materials.

Photochem **2022**, *2*, 272–298. <https://doi.org/10.3390/photochem2020020>

Academic Editor: Youngku Sohn

Received: 8 March 2022

Accepted: 21 March 2022

Published: 30 March 2022

Publisher's Note: MDPI stays neutral with regard to jurisdictional claims in published maps and institutional affiliations.



Copyright: © 2022 by the authors. Licensee MDPI, Basel, Switzerland. This article is an open access article distributed under the terms and conditions of the Creative Commons Attribution (CC BY) license (<https://creativecommons.org/licenses/by/4.0/>).

1. Introduction

Renovation for cleaning and renewing solar energy in the form of stored chemical energy has been considered a practicable and viable approach in order to face the main issues resulting from exhausting fossil fuels and using environmentally polluting materials. In 1972, researchers presented cleaning H₂ energy, which might be generated through water splitting by employing a photoelectrochemical (PEC) cell associated with TiO₂ photoanode [1]. Heterogeneously joining photocatalysis and electrochemistry is considered a synergistic strategy for efficiently achieving the conversion of solar energy [2,3]. In an ideal PEC system, the semiconducting photoelectrode becomes a basic counterpart, thereby capturing solar light as well as promoting oxidation and reduction reactions, such as water splitting [4–6], efficient CO₂ reduction [7,8], and N₂ specification [9,10].

During light irradiation, a typical semiconducting photoelectrode may be activated through photons possessing the equivalent or higher energy than the bandgap energy. As a result, photogenerated holes reside in the valence band, whereas photogenerated electrons are generated and isolated during picoseconds, afterward jumping toward the conduction

band (CB). The photo-induced charge carriers are afterward speedily accelerated toward the interfacial contact established between the photoelectrode and an electrolyte, supported by an intrinsic energy band configuration associated with an external electric field [11]. The photogenerated negative charges are triggered with reduction reactions, such as that of the hydrogen evolution reaction (HER), with a CO₂ reduction, as well as N₂ fixation. The relevant positive charges alternatively contribute to oxidation reactions similar to that of the oxygen evolution reaction (OER) and organic pollutants deprivation. Specifically, in large-scale basis applications for solar-dependent water splitting, there may be a PEC system required for possessing a higher energy conversion performance, greater HER and OER reaction speeds, prolonged stability, operating safety, and lower cost. To date, despite the great efforts that have been undertaken for approaching future targets, the achievements in catalytic efficiency have been considered inadequate for practical applications [12–16].

Thus, developing optimum energy efficient materials, thereby achieving a deep understanding of the basic principles corresponding to photochemical conversion and electrocatalytic mechanisms for a PEC system, has been suggested as being indispensable for efficiently fabricating high photoelectrodes for a solar dependent water splitting system [17]. Moreover, to increase the efficiency in relation to PEC water splitting, recent advances into two dimensional (2D) energy candidates, such as graphitic carbon nitrides (GCNs) [18], transition metal dichalcogenides (TMDCs) [19], layered double hydroxides (LDHs) [20], layered bismuth oxyhalides [21], and MXenes [22], have progressed over the recent years. When comparing conservative semiconducting photoelectrodes inherited with the usual limitation, showing a lower availability relating to active sites, the 2D layered-photoelectrode characteristic is actively explored for exposed edges associated with atomic imperfections, thereby proving to be favorable for PEC water splitting. Experimentally and theoretically, the outcomes have revealed that corresponding to an ultrathin 2D structure unified with a reduction in thickness could grant a higher exposing surface area with abundantly active sites for atoms. Meanwhile, atoms inside the surface might come closer toward the surface of ultrathin atomic layers, which facilitates the contacting area that exists among the catalysts and reactants [23–27].

On the other hand, the other exposed active sites could be exploited toward surface-functionalized catalytic responses. To add amusing surface faults, the unsaturated atoms and vigorous edges could be generated to form an ultrathin layered geometry. Consequently, to design a typical 2D layered photoelectrode by obtaining efficient light-capturing and charge separation, along with quick reaction kinetics for increasing the PEC water splitting efficiency, an agenda has been created for prominent research and developing efforts. No doubt, it has become familiar for achieving superior graded photoelectrodes, and the efficient electrocatalyst/co-catalyst has proven to be an indispensable counterpart of a PEC system. Generally, a suitable electrocatalyst might be offered for a PEC system in the form of a co-catalyst for accelerating photoelectrocatalytic reactions and improving the photo-induced charge isolation and carriage performance carried out at junctions/interfaces that exist among a co-catalyst with a light gathering semiconductor [28–30]. In previous periods, the proton reducing co-catalysts, such as noble metals [31], metallic sulfides [32], metallic phosphides [33], and oxidizing co-catalysts, such as IrO_x [34], CoO_x [35], Co₃(PO₄)₂ [36], CoCuO_x [37], and WO₃ [38], have been extensively established to be water-reducing and water-oxidizing reactions. Furthermore, individual merits belong to strengthening the interfacial contact among supportive 2D photoelectrodes and electrocatalysts, involving integrating photoelectrode and electrocatalyst systems, which could be introduced successfully [39].

In this mini-review, we aim to provide an overview of the PEC energy conversion of 2D materials, such as GCNs, TMDCs, LDH, MXenes, as well as their co-catalysts, etc. The PEC mechanisms have been discussed along with their catalytic performances. Furthermore, the improvement strategies, including heterostructure construction, and surface functionalization have also been included. Finally, the present issues and challenges have been acknowledged for facilitating future research in PEC water splitting.

2. 2D Materials for PEC

Because of its distinctive atom-thick 2D structures and unique physicochemical characteristics, graphene has been applied in many fields, including science investigations and technological applications after its discovery [40–42]. Encouraged by its excellent performance, more and more attention has been paid to synthesizing various kinds of graphene derivatives and corresponding inorganic analogs via various programs. Typically, a large number of ultrathin nanosheets, such as graphene, g-C₃N₄ [43], black phosphorene [44], TMDCs, oxides, etc., have been successfully synthesized by atomic layer deposition and liquid exfoliation methods as described in Table 1. The atom-thick layered ultimate 2D anisotropy structure composed of atomic layers is an ideal material for basic scientific research and a basic building block for designed assembly into equipment. Especially because of difficulty and limited adjustability in enlarging the bandgap of graphene used in semi-conducting devices and applications, more and more studies have been focused on these intrinsically semiconducting non-graphene 2D materials. For applications, several primary factors are responsible for the intensified PEC performance of photoelectrodes-ultrathin 2D layer materials compared to the corresponding bulk structures [45,46].

Table 1. Recent report on the 2D materials for PEC.

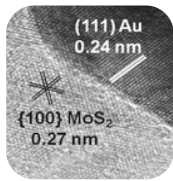
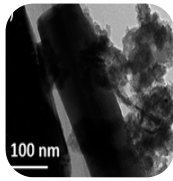
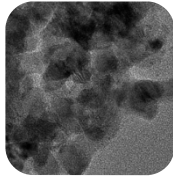

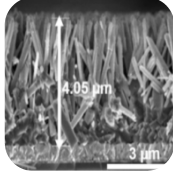
Sample	Synthesis Method	Achieved Product	Performance	Morphology	Ref.
Au-MoS ₂	Li-exfoliation (for MoS ₂ nanosheets) cysteine-linking strategy (for Au-MoS ₂)	H ₂ and O ₂ (water splitting)	N/A		[47]
MoS ₂ nanosheet/ZnO nanowire	N/A	HER	27.69 μmol		[48]
α-Fe ₂ O ₃ /BiVO ₄ /MoS ₂	Dip-coating process (for α-Fe ₂ O ₃ /BiVO ₄), liquid-phase exfoliation (for MoS ₂)	H ₂ and O ₂	6.5 μmol cm ⁻² of H ₂ and 22.3 μmol cm ⁻² of O ₂ after 2 h.		[49]
Ag-decorated vertically aligned 2D MoS ₂ on graphene	MOCVD and Thermal evaporation	Water splitting	N/A		[50]
TiO ₂ /CdS/MoS ₂	Chemical bath deposition (for TiO ₂ /CdS), and chemical exfoliation (for MoS ₂)	Water splitting	Photocurrent density of 3.25 mA/cm ₂ at 0.9 V vs. RHE (0 V vs. Ag/AgCl)		[51]

Table 1. Cont.

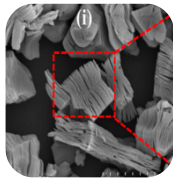
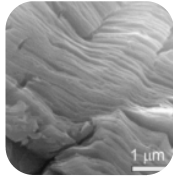
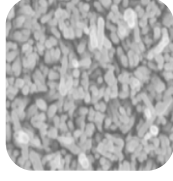
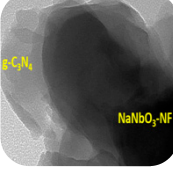
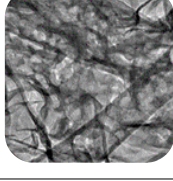
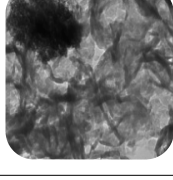
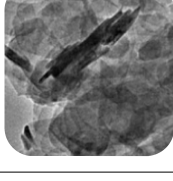
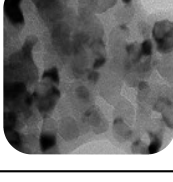
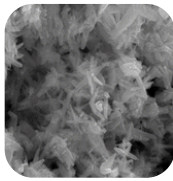
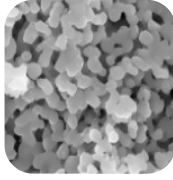
Sample	Synthesis Method	Achieved Product	Performance	Morphology	Ref.
ZnO/Ti ₃ C ₂ and Ti ₃ C ₂ /ZnO	HF etching (for MXene) and RF magnetron sputtering (for Ti ₃ C ₂ /ZnO)	Water splitting	ZnO/Ti ₃ C ₂ photocurrent generation (2.0×10^{-4} A/cm ²), Ti ₃ C ₂ /ZnO (1.75×10^{-4} A/cm ²)		[52]
Fe-TiO ₂ /Ti ₃ C ₂ T _x	HF etching (for MXene), hydrothermal (for Fe-TiO ₂), and electrophoresis (for Fe-TiO ₂ /Ti ₃ C ₂ T _x)	Water splitting	1.23 mA cm ⁻² at 1.23 V vs. RHE		[53]
α-Fe ₂ O ₃ /MXene	Hydrothermal and annealing	Water splitting	N/A		[54]
g-C ₃ N ₄ /NaNbO ₃	Hydrothermal and chemical solution route	Photoanode	Photocurrent density 12.55 mA cm ⁻²		[55]
N-deficient porous C ₃ N ₄ nanosheets and NiFe-LDH/NG	Hydrothermal and chemical exfoliations	HER and OER	Photocurrent density 162.3 μA cm ⁻²		[56]
g-C ₃ N ₄ /Au-SnO ₂	Hydrothermal and calcination	Degradation of RhB and water splitting	N/A		[57]
CoMn-LDH@g-C ₃ N ₄	Co-precipitation	OER and HER	Photocurrent density of 10 mAcm ⁻² at 1.56 V and 100 mAcm ⁻² at 1.82 V		[58]
g-C ₃ N ₄ @NiO	in-situ solid-state heat treatment	OER and HER	Photocurrent density 20 mAcm ⁻² (for OER) and 10 mAcm ⁻² (for HER)		[59]

Table 1. Cont.

Sample	Synthesis Method	Achieved Product	Performance	Morphology	Ref.
C ₃ N ₄ -CoSe ₂	Combustion technique (for C ₃ N ₄), hydrothermal (for C ₃ N ₄ -CoSe ₂)	H ₂	Photocurrent density −4.89 mAcm ^{−2} at “0” V vs. RHE		[60]
Fe ₂ O ₃ /BiVO ₄ /NiFe-LDH	Electrodeposition method	Water splitting	N/A		[61]

2.1. PEC Features

- (I) Multiple scattering and reflection within the cavities between adjacent 2D nanomaterials can improve light absorption, which occurs at the interface of a solution/electrolyte junction.
- (II) The edges of a CB and valance band (VB) would transform into H₂ reduction and O₂ oxidation electric potentials, respectively, with a decreasing nanosheet thickness, resulting in boosted thermodynamic impetus and charge transfer at the interfacial PEC water splitting.
- (III) The charge transfers at the solution/electrolyte junction interface can be promoted by the nearly all-surface-atom structure of 2D materials.
- (IV) In 2D materials, the decoupling of light absorption and charge isolation could allow the synchronous enhancement of charge transfers and adequate light absorption. Simultaneously, the interior electric field produced across the nanosheets can improve the charge isolation of the photogenerated electron-hole pairs.

2.2. MXenes

Familiar 2D materials also involve metal-free GCNs and TMDCs materials showing a great potential to fabricate superior-quality photoelectrodes, whereas there has been keen interest for the newly introduced layered MXene architectures to be strongly involved in assembling PEC systems for water splitting. Specifically, MXenes are considered a new and talented family member containing nearly 60 varieties of 2D metal carbides, nitrides, or carbonitrides, which are exploited to construct a variety of electrodes for supercapacitors, photoelectrocatalysis, and photovoltaics [62–64].

To date, MXenes have been demonstrated to possess various exceptional compensations for improving PEC efficiency. For example, various unsaturated metal locations (e.g., Ti, V, or Nb) have been explored to form 2D layer architectures, thereby resulting in higher redox reactivity than single-elemental carbon species. Additionally, hydrophilic functional groups, such as -OH and -O, reside in the form of dangling bonds over the MXene's surface, becoming advantageous for bonding with the diverting semiconductors and stabilizing 2D MXenes in an aqueous media for a prolonged term. In contrast, MXenes exhibit outstanding metallic conductivity analogous to graphene, thereby facilitating the confirmation toward efficient charge transfers. Occupying excellent properties, the 2D MXenes present as a promising candidate for constructing photoelectrodes [12–16,65–67]. Similar to graphene, monolayer MXenes occupy a hexagonal lattice associated with the rhombohedral unit cell. Whereas the side view depicts as tri-layer sheets unified with monolayer MXenes, containing two TM layers sandwiched with one X layer, caused by the function in the form of active catalytic sites toward the HER; however, MXenes resources as HER electrodes need a greater overpotential water splitting [68]. Hence, incorporating

MXene's photoelectrodes as newly activated constituents have become a feasible strategy to overcome the above shortcomings.

Currently, nanocarbons are encapsulated in MXenes-based systems, which can promote robust interfacial coupling with an improvement in separation and injection performance in favor of photogenerated charge carriers [69–74]. For instance, Qiu et al. have reported a carbon encapsulation approach for stabilizing 2D Ti_3C_2 -MXenes and constructed a ranked $\text{MoS}_2/\text{Ti}_3\text{C}_2$ -MXenes with the association of a C heterojunction, thereby exhibiting exceptional HER efficiency with high structural stability [75]. $\text{MoS}_2/\text{Ti}_3\text{C}_2$ -MXene@C showed a low overpotential of 135 mV with 10 mA cm^{-2} in a $0.5 \text{ M H}_2\text{SO}_4$ solution, Figure 1a,b. The onset potential at -20 mV toward the HER was close to commercial Pt/C, and the Tafel slope was reduced to 45 mV dec^{-1} compared with bare Ti_3C_2 -MXene, Figure 1c. Figure 1d shows the $\text{MoS}_2/\text{Ti}_3\text{C}_2$ -MXene@C exhibited a steady current density associated with a constant potential (130 mV) during a prolonged time of 20 h [76].

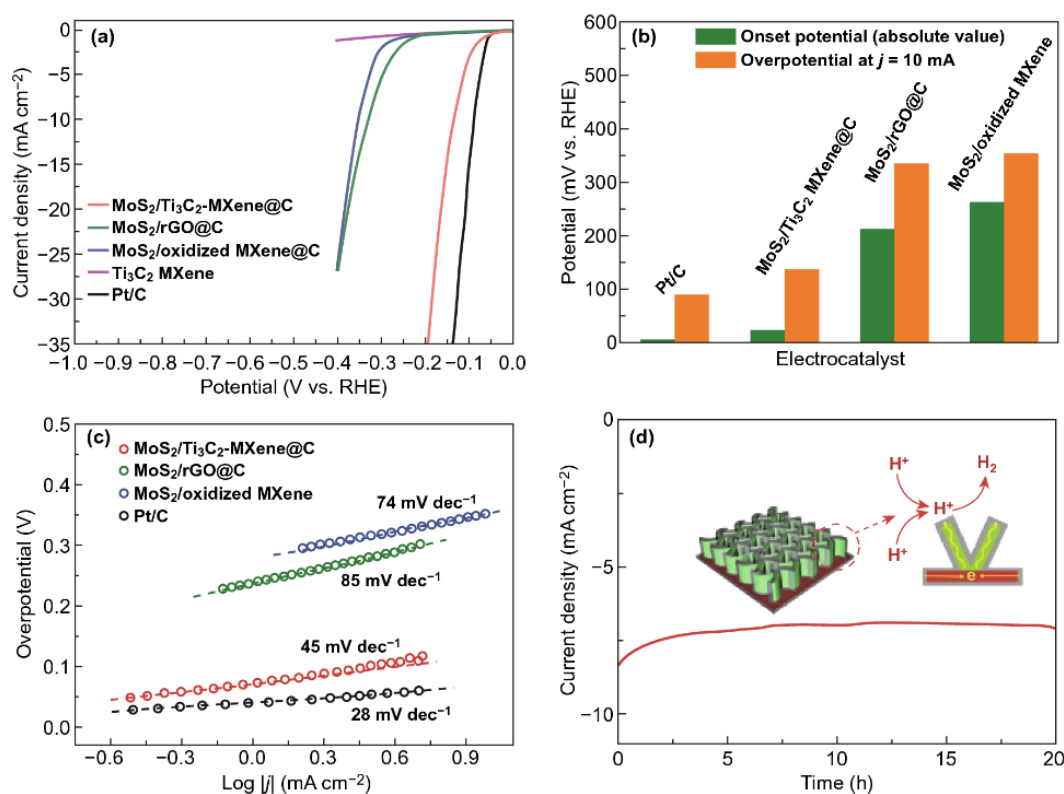


Figure 1. (a) Polarized profile. (b) Onset potential and overpotential. (c) Tafel graphs. (d) Time-based current density graphs associated with overpotential as 130 mV of $\text{MoS}_2/\text{Ti}_3\text{C}_2$ -MXene@C. Reproduced with permission from Ref. [76]. John Wiley & Sons, 2017.

Further, Zhang et al. have prepared cobalt-topped carbon nanotube (CNT)/ Ti_3C_2 nanosheets using ZIF-67 as a precursor [77]. ZIF-67 was converted into Co-CNTs by a pyrolysis procedure in the presence of layered Ti_3C_2 conductive supports. Co-CNT/ Ti_3C_2 nanosheets displayed an efficient electrocatalytic performance allied with enhancing stability related to commercial Pt/C in HER, which is attributed to the richer Co-N/C active sites, graphitization, and high surface area. The observed results indicate that 2D MXene/nanocarbons are undoubtedly considered as candidates for photocathodes in PEC systems toward efficient renewable energy resources.

2.3. Transition Metal Dichalcogenides

Layered TMDCs offer much more active centers and thickness-relied electronic structures, which favors the conversion of solar energy to produce hydrogen energy. Normally, TMDC structures, denoted as MX_2 (M: transition metals, X: S, Se, and Te), have more than

40 varieties of stabilized 2D materials with similar structures [78], which are usually made of X-M-X layers connected via van der Waals forces. Nevertheless, the atomic compositions have a great influence on the electronic properties of TMDC materials. For example, MoS₂ and MoSe₂ show semiconducting behaviors, WTe₂ and VS₂ belong to the semimetals, and TaS₂ and NbS₂ are metals. Meanwhile, the optoelectronic properties of TMDCs materials are also strongly affected by their atomic layer numbers. For example, the monolayer MoS₂ has a direct bandgap of 1.9 eV, and the corresponding bulk structure has an indirect bandgap of 1.3 eV [79]. Moreover, the semiconducting 2H-MoS₂ transforms to metallic 1T-MoS₂ with a decreasing atomic layer number that has been verified, which is availed for accelerating the motivation of photogenerated charge carriers. Chen et al. reported that nanostructured MoS₂ possessed a higher photocurrent density than bulk MoS₂ for PEC-HER [80]. The surface defects of nanostructured MoS₂ also play an important role in determining the whole activity of the water splitting reaction with photoelectrodes. By the method of in situ corrosion with bulk MoS₂, the formation of surface defects resulted in decreasing photocatalytic activity, but these produced edge sites that could enhance the performance of electrocatalytic HER. The coordination number of S atoms has an obvious influence on catalytic activity; mono-coordinated S atoms exhibited higher activity than double-coordinated S atoms. Note that three-coordinated S atom support showed no photocatalytic activity. With the presence of photogenerated electrons, the H⁺ species was easily reduced to H₂ over the active S atoms, which can vigorously bond to H⁺ in a lactic acid solution [81]. Nanosized MoS₂ with more exposed edges could provide excellent HER activity in a photochemical/PEC reaction system. Therefore, 2D nanostructured TMDCs catalysts have been generally used in recent decades as active components to assemble the integrated photoelectrodes applied in PEC water splitting reactions [82–86].

However, the speed of photoproduced charge carrier transportation is very fast, and the produced electrons and holes would be recombined in a very short time, thus the PEC performance of 2D TMDCs photoelectrodes for water splitting would decrease sharply [87,88]. To improve the PEC activity of 2D TMDC-based photoelectrodes, some carbon nano-materials have been imported to enhance the isolation and transfer of photoproduced charge carriers [89]. As shown in Figure 2a, p-n MoS₂/N-doped cGO heterojunction has been fabricated through an aerosol process in a furnace with a temperature of 900 °C [90]. The N-doped cGO/MoS₂ hybrid gave a lower overpotential of ~100 mV vs. RHE, a higher photocurrent density, and a smaller Tafel slope than a commercial MoS₂ (Figure 2b,c), which was mainly due to the generation of a localized p-n heterojunction in a N-doped cGO/MoS₂ hybrid that could largely promote the separation of photoproduced charge carriers. Then, a RGO/CdS/MoS₂ hybrid was synthesized to investigate the effects of charge transfer behavior and the crystal structure of MoS₂ in a 2D photocathode on a solar-driven HER [91]. Because of intimate contact between the S atoms in CdS/MoS₂, the intense electronic interaction between MoS₂ and RGO could be enabled, which is available for the isolation of a photogenerated charge, transfer with a higher charge density, and a lower resistance in the location of a solid–solid interface, thus impelling the PEC-HER activity.

Moreover, carbon dots (CDs) with a size less than 10 nm have been used in modifying TMDC-catalyzed photoelectrodes due to their uniquely remarkable π -conjugated system, which can enhance the speed of electron transfer between TMDCs and CDs [91–93]. For instance, CDs modified MoS₂ nanosheets have been synthesized via a hydrothermal method [94]. Under visible light irradiation, the CD-modified MoS₂ has an excellent performance (Tafel slope of 45 mV dec⁻¹ and an overpotential of ~125 mV at 10 mA cm⁻²) with an enhancing HER capacity, which was ascribed to the decreasing number of S⁴⁺ and an increasing amount with S₂²⁻ and S²⁻ sites that would accelerate the speed of charge carriers shifting between the CDs and MoS₂. Furthermore, the CDs/MoS₂ exhibited excellent stability in a solution of 0.5 M H₂SO₄. Simultaneously, the time of duration with irradiation of visible light also affected the HER activity, which was ascribed to the expansion of number reduction with MoS₂ edges and surface defects.

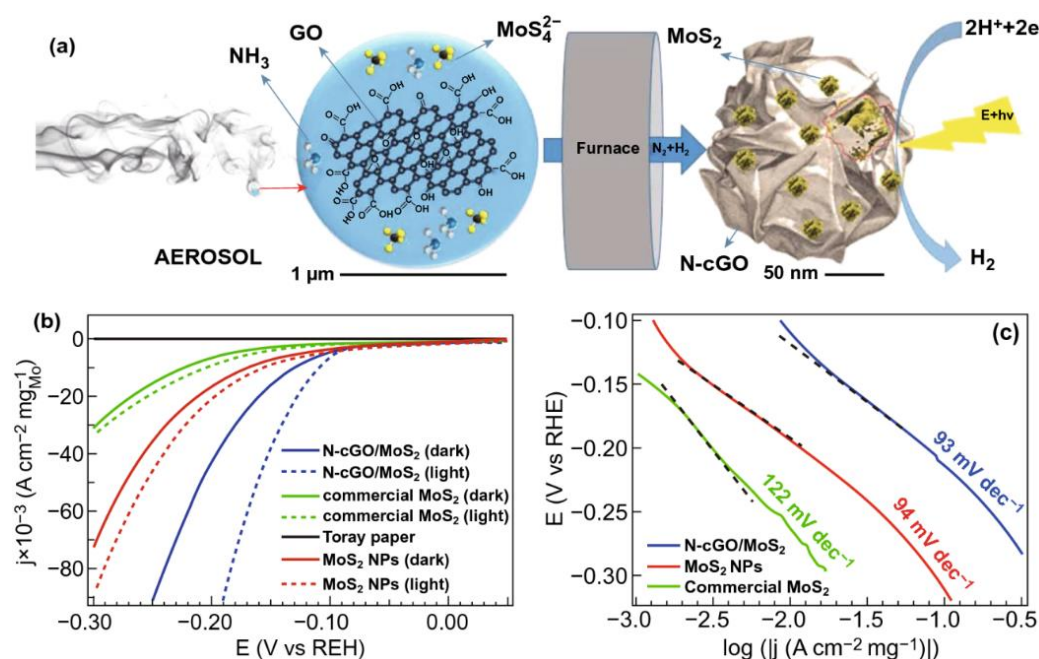


Figure 2. (a) Fabricated scheme for N-cGO/MoS₂. (b) Polarized images during dark and light illumination. (c) Tafel curves. Reproduced with permission from Ref. [90]. American Chemical Society, 2015.

2.4. Graphitic Carbon Nitride

The layered GCNs have received great attention, being 2D photocatalytic materials because of possessing facile synthesis, a lower cost, and elongated stability. Specifically, the remarkable bandgap of ~2.7 eV associated with suitable band locations favors GCNs as an attractive candidate toward water splitting [95–97]. Moreover, sunlight aimed toward energy transformation performance for graphitic carbon nitride photocatalysts has been considered unsatisfactory because of a limiting light gain capability, an excessively recombined photogenerated charge carrier, slow charge carrier transportation performance, and slowly interfacial reaction dynamics toward PEC water splitting. To overcome the aforementioned unsuitability, nanocarbons have been introduced in the form of co-catalysts and have been greatly explored in the last era. Being zero-dimensional carbon, CDs were decorated onto the surface of GCN by rendering π - π stacked interactions, thereby resulting in a narrowing bandgap with the enhancement of a light response [98,99], and the heterojunction of CDs/GCN by van der Waals exhibits a high conductivity, thus the separating performance of photogenerated electron-hole pairs at the interfacial contact of heterojunction is largely enhanced [100].

For example, Kang et al. have reported the coupling of CDs with porous GCN collectively with negative surface charges to boost up quantum capabilities moving toward an optimum efficiency of 16% as 420 nm, with the combination of a whole solar energy changing ability of 2.0% with AM 1.5G illuminated solar conversion energy [101]. Next, Guo et al. have prepared a protonated g-C₃N₄/CDs (p-CN/CDs) hybrid photoanode through utilizing an electrostatic attraction route. The photoanode has exhibited an enhancing anodic photocurrent density of 38 μ A cm⁻² with 1.0 V vs. an RHE with incident photon-to-current efficiency (IPCE) of 7.0% with 420 nm illuminated with AM 1.5G, that is turned into two and three times greater than that of pure p-CN [102]. The observed CB potential showing a -0.59 eV value for p-CN/CDs demonstrates the remarkable thermodynamical advantage of PEC-HER. On comparing with CDs that may supply merely point-to-point interfacial contact into the heterojunction, the coupling of GCN nanosheets connecting with alternative carbon materials (e.g., 2D graphene) may result in an increment in the contacting area in favor of quick charge transfers and then an enhanced PEC performance.

To date, a layered CN-RGO photoelectrode containing a large porous structure has been prepared [103], which has supplied lengthy electron diffusion touching a 36 μm , greater surface area, and with a higher light-response limit. Due to the aforementioned merits, IPCE for optimizing a CN-RGO photoanode has been impressively considered at 5.3% with 400 nm and a redshift beginning wavelength at 510 nm. Moreover, the photocurrent density belonging to the CN-RGO was valued at $75 \mu\text{A cm}^{-2}$ with 1.23 V vs. RHE in the absence of a hole-scavenging-layer, thereby being 20 times higher than that of pristine CN. At the same time, the quantum efficiency externally approached as 5.5% with 400 nm. Being an efficient charge transfer bridge, an active role of the RGO inherited with an outstanding conductivity may facilitate photo-induced electron transfers, extracted by GCN toward the substrate, which enhances the PEC-HER performance.

Further, Leung et al. have presented a RGO-derived g-C₃N₄/Ni foamy nature photoanode containing a heterostructure of g-C₃N₄ and RGO, which showed an improving PEC-HER efficiency [103]. The optimizing photoanode as a g-C₃N₄/RGO-Ni with a foamy nature has been explored with a constant transitory photocurrent density of $0.5 \text{ mA}\cdot\text{cm}^{-2}$ with 0.4 V vs. an SCE associated with a high H₂ creation rate of $6.0 \text{ mmol h}^{-1} \text{ cm}^{-2}$, which was 2.5 times greater than those of pure g-C₃N₄, respectively. Illuminated with a visible light, photo-induced electrons have been created over g-C₃N₄, and therefore may migrate quickly toward an RGO with Ni foamy nature toward H₂ evolution depending upon a strong involvement with g-C₃N₄ and RGO. Further, predictable GCN/RGO systems and a GCN/RGO hybrid heterostructure have also been designed toward efficiently high PEC water splitting. Currently, a g-C₃N₄/N-doped graphene/2D MoS₂ (CNNS/NG/MoS₂) photoanode has been prepared by employing a superficial sol-gel route [104]. Initially, the CNNS/NG composite was fabricated following one step of urea pyrolysis with GO, therefore, N-contained chemical substances have been unconfined through urea polycondensation, which in turn results from fractional reducing along with N-doped GO.

MoS₂ nanosheets have been offered in the form of a CNNS/NG hybrid through employing a hydrothermal approach for the formation of a CNNS/NG/MoS₂ hybrid. The ideal 2D/2D construction contains NG, which has been carried out in the form of a charge transfer channel to accelerate electron transformation existing among g-C₃N₄ and MoS₂, whereas g-C₃N₄ has been utilized efficiently to harvest sunlight because of its belonging to a reasonable bandgap. During the same period, the layered MoS₂ had an increased light absorbance capability, thereby promoting electron-hole pair parting and transferring corresponding with a NG/MoS₂ interfacial contact, and the provision of exposing active locations owing to the PEC-HER. Hence, the aforementioned PEC system has been offered with a wide harvesting range of light and a shortening charge diffusion length, along with an enlarging affiliated area toward highly effective PEC water splitting.

A CNNS/NG/MoS₂ heterojunction has also presented a substantial improvement in photocurrent density showing $37.6 \mu\text{A cm}^{-2}$ with incorporating NG possessing 1.46- and 3.43-times greater result as compared to CNNS/MoS₂ ($25.7 \mu\text{A cm}^{-2}$) and CNNS ($11 \mu\text{A cm}^{-2}$) with 0.9 V, respectively. Moreover, an ideal 2D single atomically thick carbon-allotrope as a graphdiyne (GDY) has been introduced as a promising candidate for photo/electrocatalysis, for attractive solar cells with charming batteries, utilizing special sp and sp² hybridized carbon atoms, and possessing moderate bandgaps of 0.44–1.47 eV, and highly charged carrier dynamics of 10^4 – $10^5 \text{ cm}^2 \text{ V}^{-1} \text{ s}^{-1}$ [105]. The GDY performed efficiently as a modifier for enhancing the PEC water splitting efficiency that was already offered in the system of GDY/BiVO₄ [106] and CdSe-quantum dots/GDY [107].

Lu et al. [108] fabricated a g-C₃N₄/GDY heterojunction as an exceptional photocathode for PEC-HER, Figure 3a. The stability of the g-C₃N₄/GDY heterojunction unified with an ultrathin layered construction (Figure 3b), and a highly charged carrier movement with a high surface has been suggested as being valuable for efficient transformation belonging to photo-induced charge carriers, thereby suppressing the reformation of photogenerated electrons and holes, and significantly revealing various active sites. This may present a greater interfacial contact lying among g-C₃N₄ and GDY, thereby providing short length

channels available for transfer of the photo-induced electron-hole pairs. The layered $g\text{-C}_3\text{N}_4$ associated with the interfacial contact of GDY has been additionally proved through following EDX elemental mapping, Figure 3d–g. Meanwhile, remarkable band alignments owing to $g\text{-C}_3\text{N}_4$ and GDY (Figure 3h), show that photo-induced positive charges emerging from the $g\text{-C}_3\text{N}_4$ may speedily move toward GDY. Consequently, photogenerated charge carriers are effectively isolated caused by an externally applied electric field. In the same dynamics, the $g\text{-C}_3\text{N}_4/\text{GDY}$ hybrid was revealed in the form of a seven-graded increment for electron tenure as $610\ \mu\text{s}$, whereas a three-graded increment was revealed with a photocurrent density of $-98\ \mu\text{A cm}^{-2}$ with $0\ \text{V}$ vs. NHE, as compared to pure $g\text{-C}_3\text{N}_4$ of $88\ \mu\text{s}$ and $-32\ \mu\text{A cm}^{-2}$ into a $0.1\ \text{Molar Na}_2\text{SO}_4$ solution, Figure 3i, that in turn revealed a $g\text{-C}_3\text{N}_4/\text{GDY}$ photoanode displaying an attractive efficiency in favor of PEC-HER.

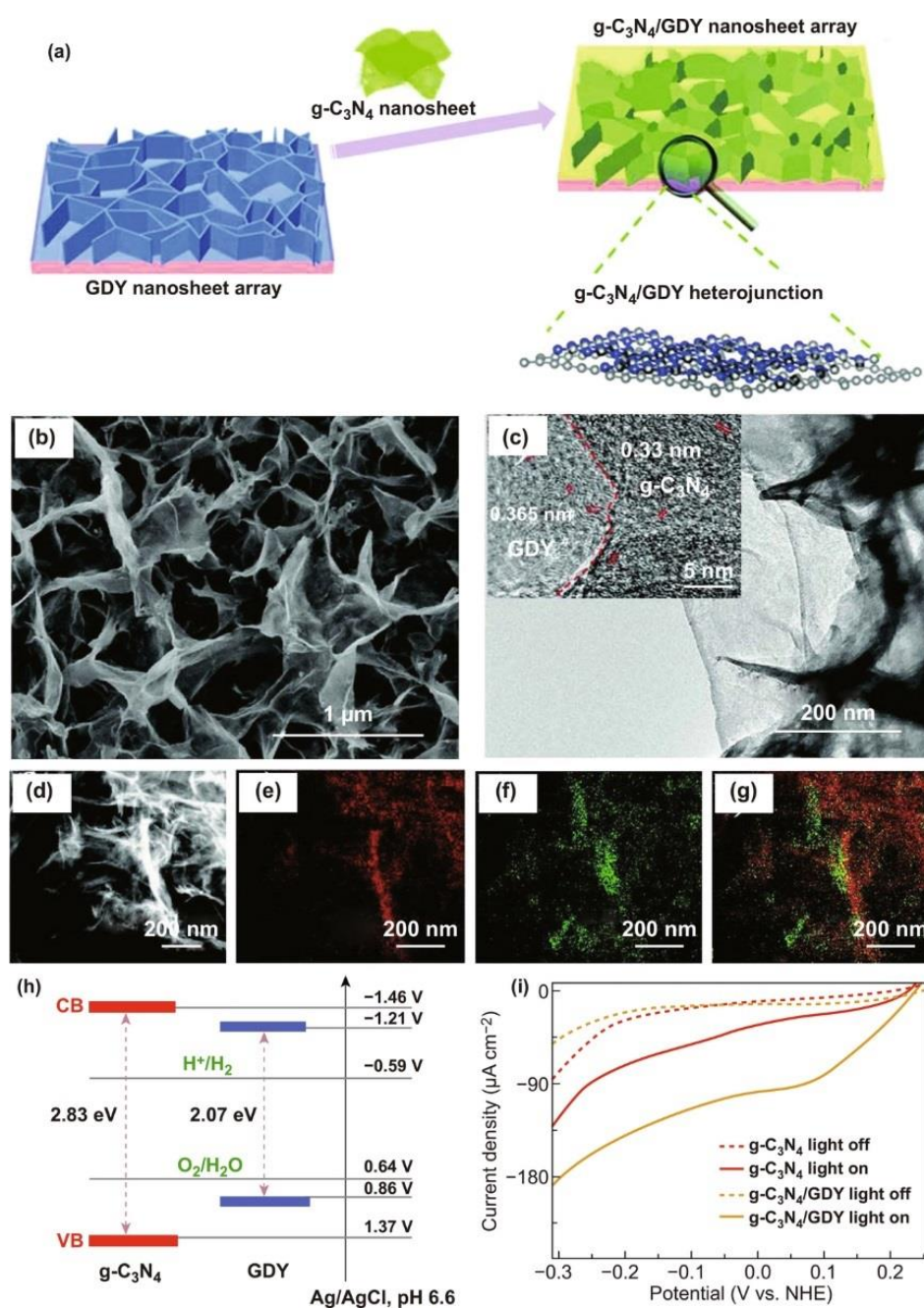


Figure 3. (a) Synthesis for $g\text{-C}_3\text{N}_4/\text{GDY}$. (b) SEM images and (c) TEM with (d–g) elemental imaging. (h) Band positions for $g\text{-C}_3\text{N}_4$ and GDY. (i) Linearly sweeping voltammetry of $g\text{-C}_3\text{N}_4/\text{GDY}$ irradiated with a light on with off. Reproduced with permission from Ref. [108]. John Wiley & Sons, 2018.

2.5. Layered Double Hydroxides

Further 2D LDHs [109–111] and metal oxides [112–114] are utilized for competent 2D photoanodes for PEC-OER. Specifically, being unique 2D materials, the layered-stacked structures of LDHs possess six oxygen sites existing at the corners, whereas one transition-metal atom exists at the mid of an octahedron of MO_6 that additionally produces 2D layered structures by involving edge atoms. Generally, LDH products are represented by the chemical formula of $\text{M}_{1-x}^{\text{II}}\text{M}_x^{\text{III}}(\text{OH})_{x+2}(\text{A}^{n-})_{x/n}\cdot m\text{H}_2\text{O}$ with brucite-nature $\text{M}^{\text{II}}(\text{OH})_2$ layers. Note that M^{II} cations can be substituted by M^{III} cations, thereby forming positive-charge layers. Thus, anions are subsequently needed to maintain charge balance. Monovalent cations (Li^+), divalent cations (such as Fe^{2+} and Ni^{2+}) [115–117], and trivalent cations, (e.g., Co^{3+} , Ti^{3+}) [118–120] have been created by forming positive charge layers with a fractional cation replacement. Accordingly, some other anions (NO_3^- , Br^- and SO_4^{2-}) have often been utilized for replacing the exact intercalation of a CO_3^{2-} anion. Further, tailored 2D nanosheets could produce active sites with full exposure, thereby elevating catalytic activity toward several reactions [121–123]. For example, LDHs have been strongly attracted in OER irradiated by light [124–126].

LDHs materials possess frequent advantages, such as having a high surface area, plentiful active sites, well-defined layered structures, flexible chemical composition through a variation of the cations ratio, stability in structure, and hierarchy of porosity, proving valuable during the water molecules diffusion process and product formation [127,128]. Furthermore, robust electrostatic exchanges between anion and cation layers offer LDHs materials with an orderly organization for the interlayer classes and tailoring toward oriented active sites, thereby accelerating the dynamics for photogenerated electrons and holes and resulting in enhancement of the OER performance [129]. Further, some researchers have noted that coupling belonging to the LDH nanosheets associated with nanocarbons significantly reduced the commencement potential related to a commercial Ir/C catalyst, which in turn increased catalytic activity through the provision of a powerful electrical route with a higher surface area [130–132].

Hou et al. have progressed a N-deficient porous nature C_3N_4 /N-doped graphene/NiFe-LDHs (DPCN/NG/NiFe-LDHs) aerogel photoanode, employing a superficial hydrothermal approach toward highly efficient PEC-OER, Figure 4a–e [56]. In a hybrid system, 3D NG has functioned in the form of an electron mediator toward shuttling photogenerated electrons and holes lying among N-deficient C_3N_4 and NiFe-LDHs, thereby leading toward enhanced separation along with transferring effectiveness for photogenerated carriers. Moreover, a DPCN/NG/NiFe-LDHs photoanode exhibited optimal configuration in favor of PEC-OER through having a uniting beneficial relevance with every component inheriting the properties for 3D aerogels. Further, the photocurrent-density owing to the DPCN/NG/NiFe-LDHs moved to $72.9 \mu\text{A cm}^{-2}$ with 1.22 V against a RHE of OER irradiated with AM 1.5G, Figure 4f, and an IPCE of 2.5% at 350 nm.

On the other hand, to accelerate quickly for interfacial mass and electron transport toward photoelectrodes while carrying out the PEC-OER process, it is considered necessary that enormous carbon-based systems be developed. For example, Wu et al. fabricated a 2D GDY photoelectrode, with an active electron mediator via an air plasma strategy [133]. Afterward, the super hydrophilic GDY was electrostatically connected with CoAl-LDH nanosheets. The CoAl-LDH/GDY photoelectrode showed an enhancement in PEC-OER performance with an overpotential of 258 mV with 10 mA cm^{-2} and a TOF of 0.60 s^{-1} with 300 mV. Meanwhile, the IPCE associated with a photocurrent density owing to a CoAl-LDH/GDY/ BiVO_4 hybrid exhibited an optimum value, which was $\sim 50\%$ with 420 nm and $\sim 3.15 \text{ mA cm}^{-2}$ with 1.23 V against RHE, respectively. The half-cell photoconversion performance of CoAl-LDH/GDY unified with BiVO_4 has been evaluated, significantly exhibiting an increment of 0.63% compared with alternative GDY-free and LDH-derived with BiVO_4 photoanodes, which was due to the drastic development of interfacial electron and mass transportation arising from the utility of a super hydrophilic GDY. The strong interaction between the GDY and CoAl-LDH resulted in an advantageous ability to absorb

water molecules lying in a neighbor of catalysts, which in turn boosted up the PEC-OER performance.

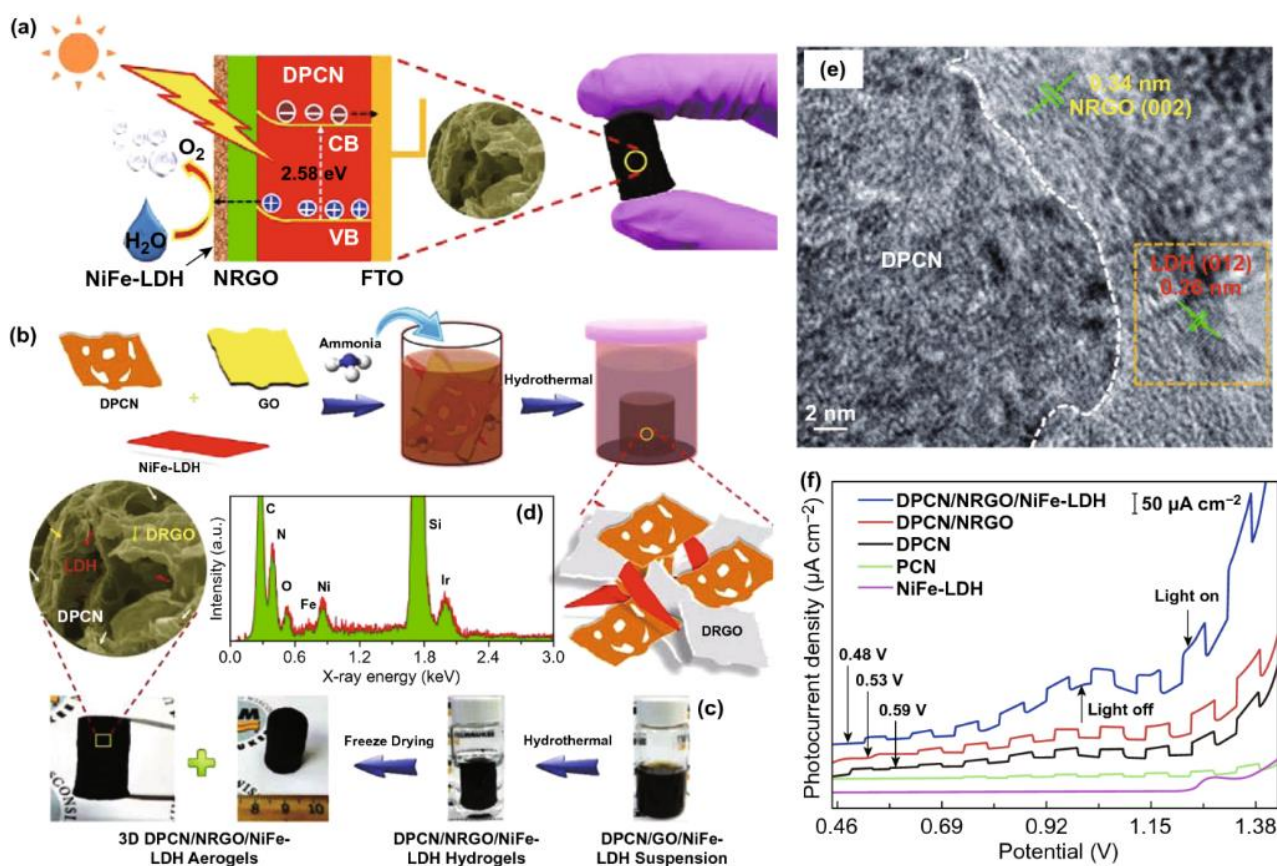


Figure 4. (a) PEC on fabricated 2D photoanode. (b) Synthetic procedure of DPCN/NG/NiFe-LDH. (c) Images for aerogel samples. (d) EDX spectra and (e) HRTEM photograph. (f) Prominent photocurrent density against external potential in chopped irradiated with AM 1.5G. Reproduced with permission from Ref. [56]. American Chemical Society, 2016.

Depending upon the optimal PEC configurations, efficient nanocarbons/LDHs systems also have displayed as energetic components that have been used supplementarily for integrating with alternative semiconductors (TiO_2 , BiVO_4 , and Cu_2O) to construct high-performing three-component photoanodes [134–141]. For instance, Ning et al. presented a more suitable approach for constructing a hybridized PEC system to introduce RGO and NiFe-LDHs over TiO_2 nanorod arrays (NAs). Moreover, this approach not only developed a separation with the transportation belonging to photogenerated electrons and holes but also enhanced the PEC-OER performance, Figure 5e,f [142]. Initially, TiO_2 -NAs were steeply grown over a FTO substrate by employing a tailored hydrothermal strategy, and layered RGO was deposited on TiO_2 -NAs. Further, layered NiFe-LDH is consistently electrodeposited over TiO_2 /RGO NAs for fabricating TiO_2 /RGO/NiFe-LDH photoanodes. Moreover, the collective experimental and computational studies have revealed that with the addition of RGO, they become strongly capable of collecting the photogenerated electrons extracted from TiO_2 because of a large work function associated with high electron mobility, Figure 5d. This electron mobility is improved, and in turn ensures the NiFe-LDH functions effectively for OER electrocatalysts. The hybrid photoanode has offered a significant improvement in the photocurrent density of 1.74 mA cm^{-2} with 0.6 V and photoconversion activity of 0.58% with 0.13 V, which is considered superior as compared with TiO_2 -based photoanodes due to a synergistic effect Figure 5a. Further, it has been evaluated in support of a charge carrier separation performance of 98% with 0.6 V over

TiO₂/RGO/NiFe-LDH NAs, which have been significantly improved at 66% with 0.6 V over pure TiO₂ NAs. Meanwhile, the charge addition performance has been improved in favor of TiO₂/RGO/NiFe-LDH, obtaining 95% along with 76% for simple TiO₂-NAs, respectively, which infers a high efficiency toward PEC-OER activity. Additionally, a ternary hybrid photoanode has been exploited on an average basis for O₂ evolution yielding 15.5 mmol h⁻¹ cm⁻² attached with a Faradaic capability of 97%, Figure 5g, which has been determined to be 1.88 times greater as compared with the TiO₂-NAs. These results have proved to introduce RGO and NiFe-LDH, revealing an apparent enhancement of the PEC-OER efficiency with a remarkable stability when irradiated with sunlight. The photo-induced electrons moved toward a RGO extraction of CB for TiO₂ with holes toward the NiFe-LDH extraction of valence band owing to the TiO₂.

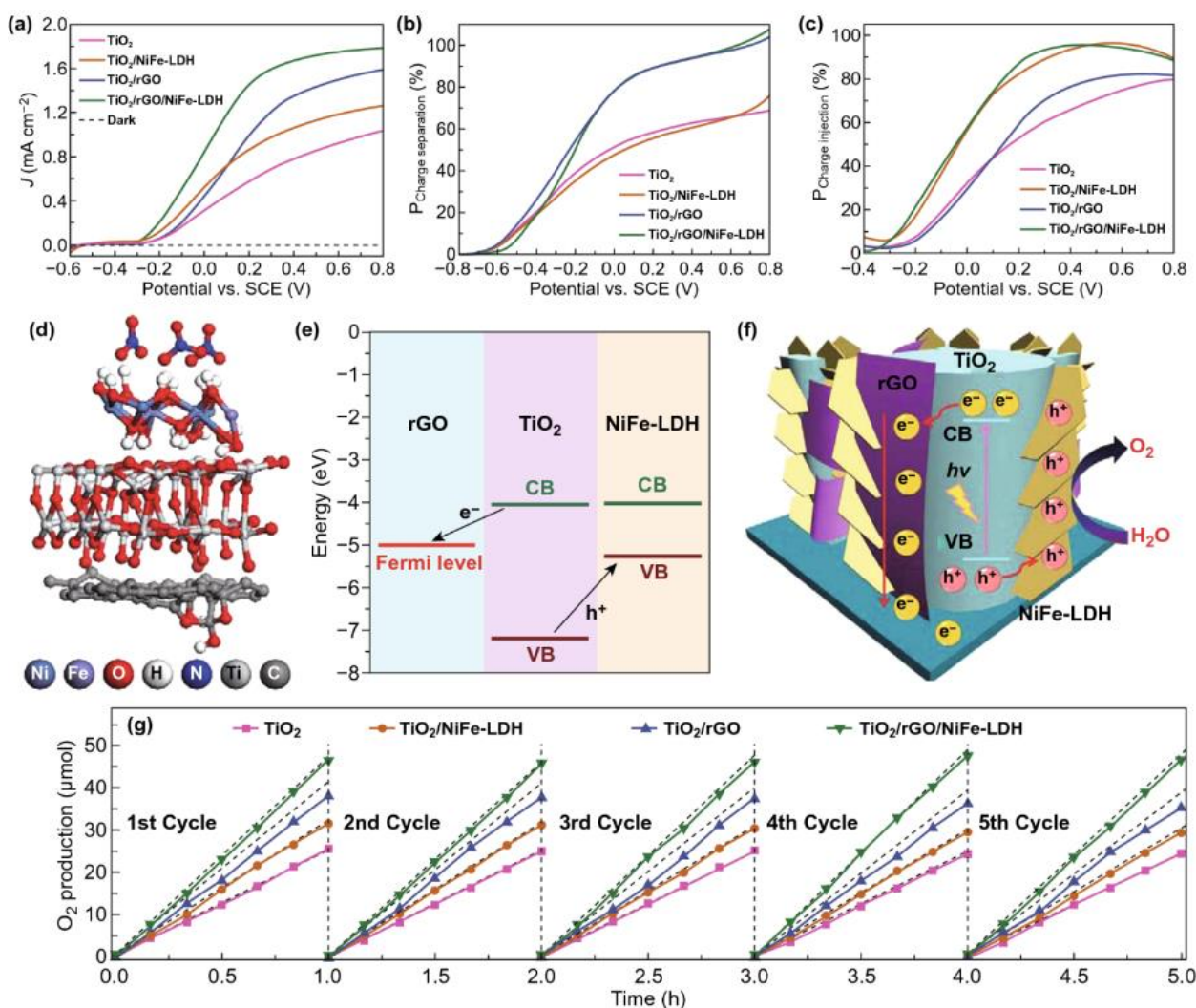


Figure 5. (a) Current–voltage graphs, (b) with charge isolation, and (c) injected performances. (d) Optimum geometry. (e) Band positions. (f) Water oxidation mechanism. (g) Original O₂ growth. Reproduced with permission from Ref. [142]. Royal Society of Chemistry, 2016.

Depending upon a synergistic strategy, Xiang et al. integrated rGO-LDH-BiVO₄ from assembling a 2D BiVO₄ photoanode with CoAl-LDHs and graphene [143]. A good enhancement of the PEC-OER efficiency was achieved by employing the hybrid photoanode. The photocurrent density and IPCE of the rGO-LDH-BiVO₄ photoanode were evaluated to be 2.13 mA cm⁻² with 1.23 V vs. the RHE and 52% with 400 nm, which were 4.0 and 2.5 times greater than those of the BiVO₄ photoanode, respectively. Consequently, these results revealed an enhancement related to the charging carrier separation performance,

whereas water oxidation kinetics may have shown the main focus in favor of RGO with CoAl-LDH. Comparable to the above-mentioned $\text{TiO}_2/\text{RGO}/\text{NiFe-LDH}$ photoanode, the resulting charge transfer channels expressively abridged the carrier dynamics length with an effective suppression toward carrier recombination. The PEC-OER performance for the photoanode could be significantly progressed through the architecture of a triadic heterostructure. On the contrary, CDs have been utilized for substituting graphene in construction with a carbon-derived NiFe-LDHs@ BiVO_4 photoanode [144]. The CDs reduce the charge transfer resistance and lower the overpotential in OER catalysis. To conclude, a ternary hybrid 2D photoanode has been explored with a significant enhancement in photocurrent associated with the IPCE value as that of NiFe-LDH/ BiVO_4 . IPCE measurements at 380 nm for BiVO_4 , NiFe-LDH/ BiVO_4 , CDs/ BiVO_4 , and CDs/NiFe-LDH/ BiVO_4 have been shown as being 19.17%, 22.97%, 24.59%, and 40.94%, respectively. During the same tenure, the CDs/NiFe-LDH/ BiVO_4 hybrid photoanode showed high transformation activity of 0.58% with 0.82 V, thereby offering an extraordinary performance of the NiFe-LDH/ BiVO_4 catalyst of 0.34% with 0.91 V, the CDs/ BiVO_4 of 0.17% with 0.99 V, and the BiVO_4 of 0.09% with 0.96 V. Furthermore, despite a charge separation performance of 66.7% with 1.23 V owing to the CDs/NiFe-LDH/ BiVO_4 possessing unattractive upgrading as compared with the alternative photoanodes, the charge injection performance was remarkably developed, increasing from 69.2% to 92.8% with 1.23 V. The result has significantly proposed that the reason for improvement in catalytic efficiency was because of a reduction in the OER overpotential as well as enhancing charge transportation kinetics. Meanwhile, the photo-induced holes may have gathered over the LDHs surface, and in turn resulted in overpotential attributed to the OER over solid–liquid interfacial contact that apparently rests on the energy barrier and reaction rate. Additionally, the decrement in OER overpotential may have recovered the PEC-OER efficiency.

3. Strategies to Improve PEC

3.1. Construction of Multicomponent Heterojunctions

For the improvement regarding PEC efficiency for photoelectrodes and to construct a multicomponent 2D-layered bulky heterojunction (BHJ) nature, photoelectrodes have also been reasonably examined [145–147]. A hexanoic acid and functionalized perylene-diimide (DHA-PDI) derived composite has been offered for the formation of a hybridized ultrathin-film type photoelectrode associated with a MoS_2 atomically layered-nature, thereby leading to the form of a valuable type-II band configuration [146]. A TEM indicated the $\text{MoS}_2/\text{DHA-PDI}$ hybridized bilayer thin film, Figure 6a. The creation corresponding to an interfacial dipole over a MoS_2 -organic interfacial contact has been significantly exhibited. It has also been proposed that type-II band alignment existing among the MoS_2 inorganic layered nature and organic DHA-PDI led toward an efficient charge isolation and an improvement in light absorption, Figure 6b.

The hybridized $\text{MoS}_2/\text{DHA-PDI}$ photoelectrode has introduced a six-fold formation into the photocurrent. With the substitution of MoS_2 for the MoSe_2 , thereby introducing a $\text{MoSe}_2/\text{DHA-PDI}$ photoelectrode, a slight increment in photocurrent was observed. This may be attributed to a great existing VB corner of the MoSe_2 , thereby creating a barrier to transfer holes toward the $\text{MoSe}_2/\text{DHA-PDI}$ interfacial contact (Figure 6b). These observations revealed great performance owing to the band alignment for the efficiency attributed to TMDC-derived heterojunctions, particularly for PEC applications. In the same way, Mattevi et al. prepared TMDCs/TMDCs type-II BHJ transparent photoelectrodes comprising of a WS_2 and MoS_2 atomically layered nature, Figure 6d,e, thereby achieving a 10 times increment in IPCE as compared to that of the sole ingredients [147]. The photocurrent produced through the WS_2/MoS_2 BHJ has been revealed as being one order of degree greater than of MoS_2 electrodes and two times greater than of WS_2 electrodes, Figure 6f. The previous increment has been ascribed to the spatially charged isolation that occurred at the moment of the WS_2 and MoS_2 layers' interfacial contact to form a type-II junction. Moreover, the exciton was dissociated, and therefore holes were migrated toward

the VB owing to the WS₂ layers during the transformation of electrons toward the CB belonging to the MoS₂ layers (Figure 6e). Owing to monolayer TMDCs, the significant occurrence was revealed during a short interval of time as 30–50 fs, that is considered as the shortest as compared to that of the intralayer reduction procedure as ca. 10 ps, belonging to a possibly trapped process through intrinsic defects as 0.6–5 ps, thereby giving a result in the form of an efficiently charged carrier isolation [148,149]. The current time for the interlayer excitons residing in the MoS₂/WS₂ and MoSe₂/WSe₂ heterojunctions was forecast along with observations taken to be in nanosecond scaling to confirm the exclusive potential for the construction of TMDCs heterostructures for applications, particularly for solar energy alteration [150].

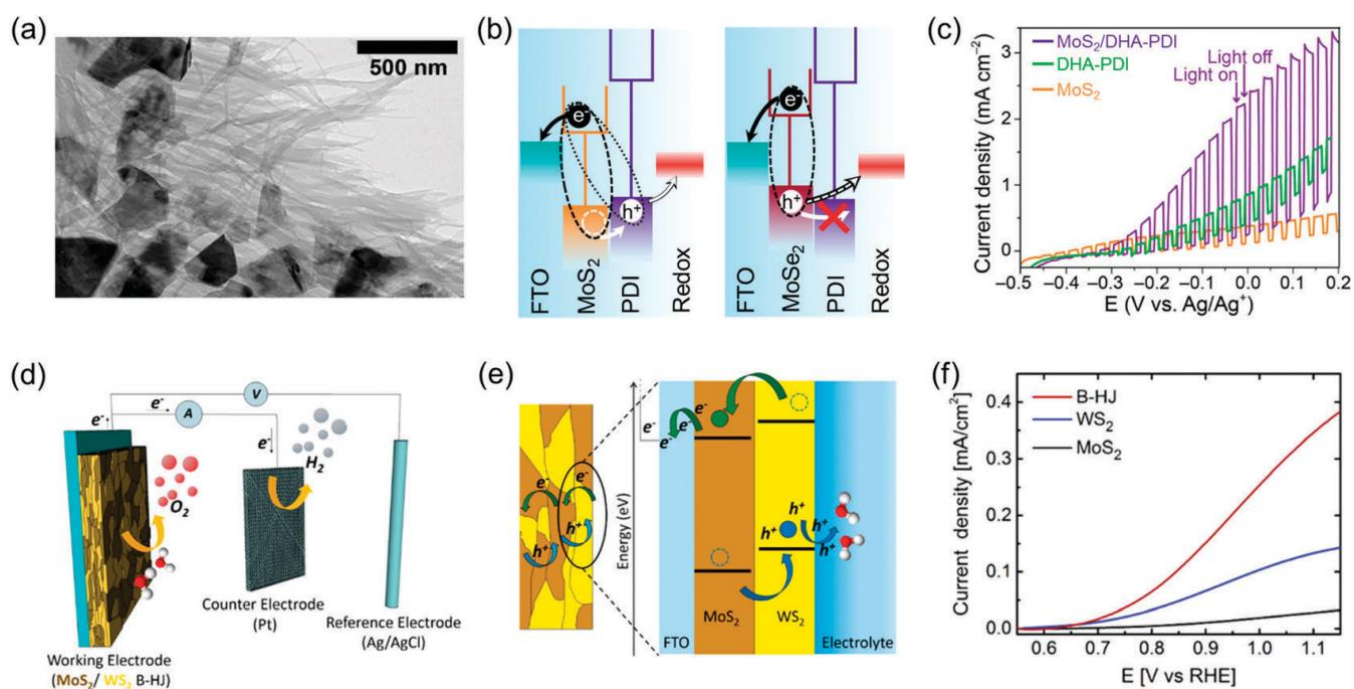


Figure 6. (a) Morphological showing of MoS₂/DHA-PDI. (b) Band position of MoS₂/DHA-PDI and MoSe₂/DHA-PDI BHJ schemes. (c) J–V graphs measuring by an I[−]/I^{3−} redox coupling during irregular (1 sun) illumination. Reproduced with permission from Ref. [146]. American Chemical Society, 2017. (d) Illustrated for various PEC cell counterparts, and (e) band geometry alignment for type-II contact associated with attributed carrier transformation. (f) PEC efficiency for BHJ photoanodes showing J–V curves. Reproduced with permission from Ref. [147]. American Chemical Society, 2017.

Ho et al. have reported an electrostatic and unified 2D hetero-layered-hybridized composite containing an atomically layered nature of MoSe₂ and ZnIn₂S₄, which has been observed for improving the visible range of light photoreactivity, and efficiently charged transformation along with close interface connection to create stability in the cycling process [151]. Concerning the band structures of ZnIn₂S₄ and MoSe₂, the photogeneration of electrons originating from the exciton for the ZnIn₂S₄ was thermodynamically excited to transfer toward the MoSe₂. This indicated that the ZnIn₂S₄–MoSe₂ hetero and layered form structure accelerated the charge carrier isolation at the interfacial contact associated with the facilitation of proton drop over the surface of the MoSe₂, caused by the regular ability of TMDC layers containing visible edge locations toward an effective decrement for activation energy revealing an overpotential concerning the redox reactions. Moreover, time resolving and steady stating PL spectra associated with an electrochemical impedance spectra (EIS), displayed spontaneous PL quenching, along with a lifetime reduction, and a decrement for the charge transfer resistance of the ZnIn₂S₄–MoSe₂ layers extracted with

a bulky ZnIn_2S_4 complement. This indicates the formation was relevant with electron transferring channels originating from the ZnIn_2S_4 toward the MoSe_2 along with a non-radiative quenching channel, caused by the resultant efficiency due to an interface charge transformation and destruction for the charge carrier recombination existing in the ZnIn_2S_4 - MoSe_2 hetero-layered form. Jointly, the ZnIn_2S_4 - MoSe_2 composite has revealed nearly a 22-fold photocurrent improvement as compared to bulky ZnIn_2S_4 under a similar environment, confirming the structure along with composition advantages of the ZnIn_2S_4 - MoSe_2 hetero-layers for promoting charge transportation as well as separation.

3.2. Surface Functionalization

Associated photosensitizer molecules have been comprehended by merely drop-casting phthalocyanine/porphyrin mixers over TMDC films [152] or dipping TMDC films into solution for 15 to 20 min [153,154]. Choi et al. presented a typically monolayered-nature WSe_2 -NiPc (Ni-oriented phthalocyanine) mechanism [153]. PL signals of WSe_2 were steadily quenched onto successive stages for 10 mM NiPc activation. During the same period, normalizing PL intensities were reduced associated with an increment in the partial surface exposure unified with NiPc, by proposing a high surface exposure, thereby leading to an increment in probability owing to the photo-induced charge carrier transport, which in turn revealed PL quenching over the NiPc activation. Additionally, the quenching PL production was totally improved at the time of removal of the NiPc molecules from the WSe_2 surfaces, which could be reactivated in the recycling of repeated times. Additionally, chemical-exfoliation with a large-area of MoS_2 ultrathin films interfaced with various porphyrin types with PEC properties have been examined [154].

It has been evaluated that photocurrents are strictly attached with HOMO and with LUMO altitudes owing to porphyrins. Through MoS_2 surface functionalization with zinc-oriented protoporphyrin IX, a 10-fold photocurrent increment was achieved. With the selection of phthalocyanine/porphyrin species with the proper band alignment relating to TMDCs, effective isolation occurred for reactive holes toward the OER and electrons toward the HER for SEJ interfacial contact [152]. The achievements exhibited magnitudes and signs owing to photocurrents that may have been anodic or cathodic, that have been explored through the concerning band energies existing among TMDCs, and the HOMO/LUMO stages of zinc protoporphyrin (ZnPP). As an example, the CB and VB edging positions for ZnPP are greater than MoS_2 and WS_2 , generating holes originated by the excitation for MoS_2 and WS_2 . It is supposed to be thermal transportation toward ZnPP and from there photoelectrons traveling from the hind contact toward a counter electrode, which in turn lead prominently to improving the photoanodic effect. Moreover, the anodic photocurrent related with the ZnPP- MoS_2 has been evaluated as being two times greater than the ZnPP- WS_2 , thereby attributed to a greater accelerating force of extraction with a higher variance with respect to the energy levels existing among MoS_2 and ZnPP. Similarly, concerning ZnPP- MoSe_2 and ZnPP- WSe_2 architecture, there is an observed cathodic photocurrent caused by the VBs of MoSe_2 and WSe_2 , reflecting levels greater than that of the HOMO energy levels of ZnPP [152]. This interfacial architecture strategy has offered novelty to improve the PEC efficiency for TMDC-dependent photoelectrodes.

3.3. Formation of Heterostructures

The merging of TMDC layers for BHJ photoelectrodes containing graphene derivatives (NG, RGO, and g- C_3N_4) for PEC applications have prominently been described [90,155–157]. Narayanan et al. have displayed the molecular foundation owing to layered ranking/stacking sequentially depending on the PEC activity rendering into a MoS_2 /graphene van der Waals vertical architecture, Figure 7 [156]. Further, they have explored the existence of MoS_2 that may influence p-type doping into graphene, thereby facilitating additional H_2 absorbance over the graphene location rather than that of the MoS_2 location, maximizing the efficiency of the graphene associated with monolayer MoS_2 , which is additionally reduced, attributed to bilayers as well as multilayers owing to the MoS_2 . Further, the graphene existence

over the monolayer MoS₂, in the form of a stacking sequence, showing the optimum photocurrent density along with beneath charge transferring resistance toward the HER, has been observed. The observations mentioned above have produced an association for a stacking sequence into PEC efficiency belonging to TMDC/graphene hybridized Van der Waal layers.

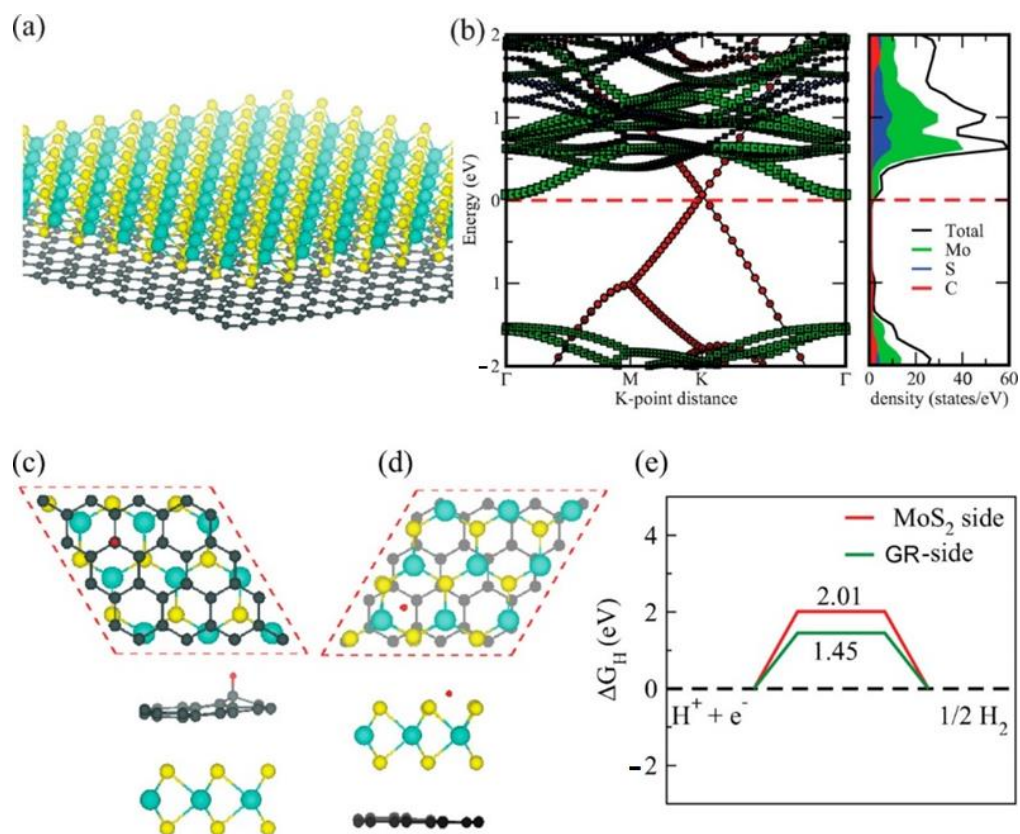


Figure 7. (a) Bi-layered heterostructure. (b) Relevant band structure and density of states. Hydrogen (red sphere) adsorption toward (c) graphene orientation and (d) MoS₂. (e) Curve for ΔG_H denoting hydrogen adsorption for both mentioned cases. Reproduced with permission from Ref. [156]. American Chemical Society, 2017.

Shin et al. [157] have examined an ideal hybrid system containing 1T-MoS₂/2H-MoS₂/2H-WS₂/RGO multi-layers. It was significantly detected for 1T-MoS₂ layers contributing to the catalytic performance of HER. The hybrid nature owing to 2H-MoS₂ and 2H-WS₂, involving various band structures, facilitates effective charge carrier dynamics facilitated with a promising band alignment. RGO nanosheets in the form of a conductively unified network to promote charge isolation have been offered. Consequently, the relevant constituents have been occasioned efficiently toward PEC efficiency for optimum, hybridized ultrathin film photocathodes. Additionally, for graphene derivatives, few-layered black phosphorus (BP), being the subject of novel research attention toward the 2D materials family, has also been associated with TMDCs such as WS₂, and has showed an improvement in photocurrent retorts at 4780 nm irradiated with near-infrared [158].

For BP/WS₂ systems, Majima et al. have presented a CB and VB edge location for BP that have been assessed as ca. ~ 0.18 and 0.52 eV vs. NHE, irradiated with near-infrared range and excitation caused by a narrowed bandgap. The narrow bandgap may essentially result in a fast charge recombination attributed to the BP. Nevertheless, due to interaction with WS₂, the electrons in the CB for BP might be proficiently included in the WS₂ layers, caused by a lower work function attributed to WS₂ indicating as 1.07 eV vs. NHE. Adequate electrons are trapped toward the WS₂, thereby reducing the protons

(H⁺) in water leading to HER. The charge isolation mechanism has been explored through PEC measurements, with an electron reduced reaction investigation as well as transitory fascination spectroscopy. Consequently, while involving ethylenediaminetetraacetic acid in the form of an artificial mediator to trap holes, the BP/WS₂ hybrids obtained a 21- and 50-times improvement in HER performance as compared to that of bare BP and WS₂, respectively. Therefore, there are benefits to consider owing to the BP/WS₂ hybridized layers behaving like photoelectrodes that are noble metal-free and irradiated close to the infrared region, along with photocatalytic materials offering novel chances while catching a wide range solar spectrum-band toward energy renovation. Collectively, the reports have identified novel routes to modulate PEC efficiency while offering novelty into TMDC layered dependent photoelectrodes associated with suggested opportunities for effective progress attributed to transparent, larger area and lower cost, solar-energy transformation devices.

4. Theoretical Aspects

H₂ and O₂ generation by splitting water is considered a sustainable solution to solve the energy crisis. The overall splitting of water includes two self-governed reactions: HER and OER at the cathodic and anodic sides, respectively. HER is a two-electron transfer process ($2\text{H}^+ + 2\text{e} \rightarrow \text{H}_2$), and OER is a four-electron transfer process (acidic condition: $2\text{H}_2\text{O} + \text{O}_2 \rightarrow 4\text{H}^+ + 4\text{e}$ or alkaline condition: $4\text{OH}^- + \text{O}_2 \rightarrow 2\text{H}_2\text{O} + 4\text{e}$). Thus, it requires that electrocatalysts should have an efficient performance in both HER and OER, being the different reaction kinetics between the two electrodes in overall water splitting. To design these bifunctional catalysts, emerging composite heterostructures may show great potential in combining the synergic effect of different components to boost catalytic performances. Therefore, a variety of composite heterostructures of 0D–1D, 0D–2D, 1D–2D, and 2D–2D have been developed in the water-splitting attributed to the electron transfer and conductivity in heterostructures that can be improved by a suitable combination of two constitutions. For example, the 0D–1D heterostructure of C₆₀ and SWCNTs can induce the intermolecular charge-transfer, [159] which trigger the inert C material to become active. Liu et al. reported the combination of a 1D-CNT with a thienothiophene-pyrene covalent organic framework (COF) for OER. It found that the charge transfer barrier from the CNT to COF at the heterointerface was tailored by the thickness of the 2D COF shell, [160] resulting in an enhanced OER activity.

Although the HER process is simpler than OER, it still challenging in an alkaline system. In an alkaline media, the HER activity is determined by the activation and dissociation of H₂O to form hydrogen intermediates ($\text{H}_2\text{O} + \text{e} + * \rightarrow \text{H}^* + \text{OH}^-$). Thus, the catalysts for HER should not only show a near-zero Gibbs free energy of the adsorbed hydrogen but also exhibit a good capacity to break the H–OH bonds effectively. Jiang et al. prepared a 0D–2D heterostructure Ru₂P/WO₃@NPC (NPC: N, P co-doped carbon), showing a superior HER performance in an alkaline media [161]. The HO–H bonds can be effectively cleaved by W atoms at the heterointerface, meanwhile the hydrogen adsorption and desorption favor at Ru sites to form a H₂ product. Further, dissimilar 2D nanosheets were investigated as multifunctional electrocatalysts in the fast kinetics and durable water splitting due to their large surface area and high redox capacity by high-speed charge separation and transfer at vertical and lateral heterointerfaces. Of note, some 2D material itself showed inferior catalytic activity or poor stability in the HER and OER due to its low density of active sites, limited electrical conductivity, and instability. Dai et al. assembled a 2D–2D EBP/NG heterostructure as an electrolyte for the overall water splitting in alkaline solutions [162]. The large work function of BP triggers the electron transfer from NG to the BP active sites, resulting in the charge redistribution at the 2D–2D heterointerface. The electron accumulated BP nanosheet not only efficiently reduced the hydrogen adsorption energy to give H₂ but also optimized the binding strength of OER intermediates to improve the OER kinetics in the overall water splitting. Note that the stability of BP was largely enhanced by an NG nanosheet in the hybrid heterostructure.

On the other hand, covalently bonded heterointerfaces can solve the weak structural stability of heterostructures through van der Waals and limited changing of the electronic property. A covalent heterostructure of NiO and Ni nanosheets onto an Ag nanowire network displayed high HER performance and catalytic stability in alkaline media [163]. The different materials were covalently bonded together to form a heterointerface, which facilitated electron migration and the separation of charge carriers through covalent-bonds. The modified electronic property of Ni and O sites near the heterointerface rendered a high intermediate affinity to OH^* and H^* species and gave a nearly barrier-free water dissociation. Furthermore, when a Pt single atom was doped at the heterointerface of the Ni/NiO, a Pt site with a locally enhanced electric field induced a higher Pt 5d occupation at the Fermi level that offered a favorable hydrogen adsorption energy. This concept of anchoring heteroatoms on an appropriate substrate can be well expanded to design efficient multi-functional catalysts.

Theoretical aspects have also provided some guidance to design bifunctional heterostructure electrocatalysts for overall water-splitting, such as (i) suitable integration of two distinct materials to generate a heterostructure, taking advantage for HER on one component and for OER on the other, and (ii) composition manipulation at the heterointerface (including doping, adding linkers, vacancies, etc.) to modify the electronic property of electrocatalysts. In one word, these aspects are aimed at turning the charge distribution at the heterointerface which modulates the intermediate binding and then boosts the kinetics of both HER/OER during overall water-splitting [164,165].

5. Conclusions, Challenges, and Future Perspective

The solar-oriented PEC significantly representing water splitting systems has been denoted as a superior faculty for the conversion of solar energy in the shape of cleaning as well as sustainable chemical energy generation. The PEC mechanisms mentioned above denote an integrated photoelectrode, thereby incorporating light-harvesting for absorbing solar energy sources while offering interlayered transformation belonging to photogenerated charge carriers associated with catalysts during the triggering of redox chemical reactions. In detailed discussion, the novelty into 2D layered photoanodes and photocathodes, especially and prominently for GCNs, TMDC, LDH, MXenes, and co-catalysts, for assembling in a collective form of photoelectrodes offering oxygen and hydrogen growth chemical reactions was reported. In addition, very intrinsic principles attributed to PEC owing to the water splitting mechanisms containing physicochemical properties for photoelectrodes, therefore involving specific catalytic reactions, have also been analyzed. The attributed interconnection among the 2D photoelectrodes is too detailed in supplementary analysis. The improvement strategies include the construction of heterostructures, surface functionalization, and formations of heterojunctions that have also been discussed.

The effective optimizing principles, such as metal-free nanocarbons as that of 0D CDs, 1D CNTs, 2D graphene as well as 2D GDYs, have been utilized in the form of electron mediators for improving the isolation and transportation proficiencies for photogenerated electrons and holes owing to high performing PEC systems for water splitting. Meanwhile, the authentic art of synthesis along with characterizations for 2D photoelectrodes hybrid-nanocarbons for highly efficient PEC water splitting has been significantly studied. In this regard, g- C_3N_4 material has been as extensively reviewed as that of photoelectrodes because of possession of an exclusive layered structure, reasonable bandgap, whereas a proper negative conduction band is attributed to HER. The g- C_3N_4 performs as a supporting material for harvesting solar energy as well as an effective electrocatalyst for driving electrocatalytic HER. To develop PEC-HER efficiency, graphene associated with CDs has been repeatedly involved in g- C_3N_4 for enhancing the isolation and transportation performance owing to photogenerated charge carriers. Similarly, for g- C_3N_4 being utilized alone, TMDC particularly of MoS_2 , and the HER catalysts too, meet a poor separation as well as a severe recombination that belongs to the photogenerated charge carriers. To avoid these difficulties, a chain of nanocarbons such as that of graphene or CNTs inherited

with a higher charge mobility in the form of co-catalysts, have been offered as solutions for assembling photocathodes, thereby exhibiting a significant progress toward PEC-HER performance. Moreover, despite emerging MXenes along with metallic conductivities and higher exposing metal sites, that exhibit strong redox activity toward HER and thereby show isolation and transportation efficiency owing to photogenerated charge carriers, there yet needs to be considerable improvement. Thus, nanocarbons such as CNTs, being co-catalysts as well as electron mediators, have been involved in MXenes for promoting the charge carrier isolation and transformation in photocathodes to enhance the PEC-HER performance that is illuminated by light.

Apart from the aforementioned $g\text{-C}_3\text{N}_4$, TMDCs, along with the MXenes for a competent HER, the LDHs are introduced as Ru or Ir-free photoelectrodes to achieve higher PEC-OER activity, caused by the LDHs materials containing transition metals such as Fe, Co, and Ni. Further, these metals enable the PEC-OER to be comparatively lower overpotentials, which in turn accelerate the water splitting. More importantly, LDH materials significantly retain a tunable chemical composition through changing ratios owing to various cations, porous-like nanostructures associated with a specific surface area, with high exposing active sites along with higher catalytic reaction rates, and a higher structural stability. Due to these qualities, the varied LDHs-based photoanodes using nanocarbons have been investigated. These aforesaid observations have explored significant performances to improve PEC water splitting as compared with that of bare LDHs photoanodes. Meanwhile, bismuth oxyhalide (BiOI) has been numerously utilized as a light absorber toward PEC-OER and because of it possessing a semiconducting nature, it shows a sufficient positive valence band, whereas photoinduced holes associated with a strong oxidative ability may substantially oxidize water for producing O_2 . Hence, these bismuth oxyhalides have been combined with layered nanocarbons, such as graphene and GDY (co-catalysts) for forming hybridized photoanodes, which in turn may achieve the targeted goal toward PEC-OER performance. Not only attractive achievements have been gained to increase the PEC-HER as well as the PEC-OER performances through the coupling of photoelectrodes along with nanocarbon co-catalysts, to date; however, the performance of supporting materials with nanocarbons for heterostructured photoelectrodes are still not completely implicit, caused by a lack of reasonable experimental suggestions along with adequate theoretical understandings. Consequently, comprehensive knowledge toward reactive mechanisms is considered as a feasible route while designing and fabricating a highly efficient performance of integrated photoelectrodes toward water splitting.

Recently, direct comparative studies of PEC-HER/OER presentations among a variety of nanocarbons-based photoelectrodes with metal clusters [166–169] have shown a fairly challenging situation due to the compositions, quantities, and testing parameters, thereby prominently affecting PEC outcomes. Therefore, there is an immense need for test principles as well as particular conditions for PEC-HER/OER to be unified in the coming years. Furthermore, the synthesis approaches owing to photoelectrodes and nanocarbons have been considered as the basic determinants toward final water splitting performances. Therefore, there should be an obligation for developing variously feasible and integrated synthetic protocols, such as that of the electrochemical or hydrothermal routes to compare and find an optimally desired material system. In all, it is a promising approach for translating the laboratory-based research and the extensive marketable applications in favor of PEC-HER/OER developments.

Author Contributions: Investigation, X.Z., C.C. and S.A.; resources, A.R. and A.A.R.; writing—original draft preparation, X.Z., S.A. and A.R.; writing—review and editing, C.C., A.R. and G.L.; supervision, A.R. and G.L.; project administration, C.C. and G.L. All authors have read and agreed to the published version of the manuscript.

Funding: This research received no external funding.

Institutional Review Board Statement: The study was conducted in accordance with the Declaration of Helsinki, and approved by the Institutional Review Board.

Informed Consent Statement: Not applicable.

Conflicts of Interest: The authors declare no conflict of interest.

References

1. Fujishima, A.; Honda, K. Electrochemical Photolysis of Water at a Semiconductor Electrode. *Nature* **1972**, *238*, 37–38. [[CrossRef](#)] [[PubMed](#)]
2. Low, J.; Yu, J.; Jaroniec, M.; Wageh, S.; Al-Ghamdi, A.A. Heterojunction Photocatalysts. *Adv. Mater.* **2017**, *29*, 1601694. [[CrossRef](#)] [[PubMed](#)]
3. Xu, Q.; Zhang, L.; Yu, J.; Wageh, S.; Al-Ghamdi, A.A.; Jaroniec, M. Direct Z-scheme photocatalysts: Principles, synthesis, and applications. *Mater. Today* **2018**, *21*, 1042–1063. [[CrossRef](#)]
4. Hisatomi, T.; Kubota, J.; Domen, K. Recent advances in semiconductors for photocatalytic and photoelectrochemical water splitting. *Chem. Soc. Rev.* **2014**, *43*, 7520–7535. [[CrossRef](#)]
5. Roger, I.; Shipman, M.A.; Symes, M.D. Earth-abundant catalysts for electrochemical and photoelectrochemical water splitting. *Nat. Rev. Chem.* **2017**, *1*, 0003. [[CrossRef](#)]
6. He, T.; Zhang, C.; Zhang, L.; Du, A. Single Pt atom decorated graphitic carbon nitride as an efficient photocatalyst for the hydrogenation of nitrobenzene into aniline. *Nano Res.* **2019**, *12*, 1817–1823. [[CrossRef](#)]
7. Wang, W.-H.; Himeda, Y.; Muckerman, J.T.; Manbeck, G.F.; Fujita, E. CO₂ Hydrogenation to Formate and Methanol as an Alternative to Photo- and Electrochemical CO₂ Reduction. *Chem. Rev.* **2015**, *115*, 12936–12973. [[CrossRef](#)]
8. Lu, C.; Yang, J.; Wei, S.; Bi, S.; Xia, Y.; Chen, M.; Hou, Y.; Qiu, M.; Yuan, C.; Su, Y.; et al. Atomic Ni Anchored Covalent Triazine Framework as High Efficient Electrocatalyst for Carbon Dioxide Conversion. *Adv. Funct. Mater.* **2019**, *29*, 1806884. [[CrossRef](#)]
9. Ali, M.; Zhou, F.; Chen, K.; Kotzur, C.; Xiao, C.; Bourgeois, L.; Zhang, X.; MacFarlane, D.R. Nanostructured photoelectrochemical solar cell for nitrogen reduction using plasmon-enhanced black silicon. *Nat. Commun.* **2016**, *7*, 11335. [[CrossRef](#)]
10. Yu, L.-L.; Qin, J.-Z.; Zhao, W.-J.; Zhang, Z.-G.; Ke, J.; Liu, B.-J. Advances in Two-Dimensional MXenes for Nitrogen Electrocatalytic Reduction to Ammonia. *Int. J. Photoenergy* **2020**, *2020*, 5251431. [[CrossRef](#)]
11. Zou, X.; Yuan, C.; Dong, Y.; Ge, H.; Ke, J.; Cui, Y. Lanthanum orthovanadate/bismuth oxybromide heterojunction for enhanced photocatalytic air purification and mechanism exploration. *Chem. Eng. J.* **2020**, *379*, 122380. [[CrossRef](#)]
12. Ikram, M.; Hassan, J.; Imran, M.; Haider, J.; Ul-Hamid, A.; Shahzadi, I.; Ikram, M.; Raza, A.; Qumar, U.; Ali, S. 2D chemically exfoliated hexagonal boron nitride (hBN) nanosheets doped with Ni: Synthesis, properties and catalytic application for the treatment of industrial wastewater. *Appl. Nanosci.* **2020**, *10*, 3525–3528. [[CrossRef](#)]
13. Raza, A.; Qumar, U.; Hassan, J.; Ikram, M.; Ul-Hamid, A.; Haider, J.; Imran, M.; Ali, S. A comparative study of dirac 2D materials, TMDCs and 2D insulators with regard to their structures and photocatalytic/sonophotocatalytic behavior. *Appl. Nanosci.* **2020**, *10*, 3875–3899. [[CrossRef](#)]
14. Wei, X.; Akbar, M.U.; Raza, A.; Li, G. A review on bismuth oxyhalide based materials for photocatalysis. *Nanoscale Adv.* **2021**, *3*, 3353–3372. [[CrossRef](#)]
15. Raza, A.; Qumar, U.; Haider, A.; Naz, S.; Haider, J.; Ul-Hamid, A.; Ikram, M.; Ali, S.; Goumri-Said, S.; Kanoun, M.B. Liquid-phase exfoliated MoS₂ nanosheets doped with p-type transition metals: A comparative analysis of photocatalytic and antimicrobial potential combined with density functional theory. *Dalton Trans.* **2021**, *50*, 6598–6619. [[CrossRef](#)]
16. Raza, A.; Qin, Z.; Ahmad, S.O.A.; Ikram, M.; Li, G. Recent advances in structural tailoring of BiOX-based 2D composites for solar energy harvesting. *J. Environ. Chem. Eng.* **2021**, *9*, 106569. [[CrossRef](#)]
17. Lei, C.; Wang, Y.; Hou, Y.; Liu, P.; Yang, J.; Zhang, T.; Zhuang, X.; Chen, M.; Yang, B.; Lei, L.; et al. Efficient alkaline hydrogen evolution on atomically dispersed Ni–Nx Species anchored porous carbon with embedded Ni nanoparticles by accelerating water dissociation kinetics. *Energy Environ. Sci.* **2019**, *12*, 149–156. [[CrossRef](#)]
18. Xie, H.; Zhang, J.; Wang, D.; Liu, J.; Wang, L.; Xiao, H. Construction of three-dimensional g-C₃N₄/attapulgite hybrids for Cd(II) adsorption and the reutilization of waste adsorbent. *Appl. Surf. Sci.* **2020**, *504*, 144456. [[CrossRef](#)]
19. Liu, J.; Li, Y.; Ke, J.; Wang, Z.; Xiao, H. Synergically Improving Light Harvesting and Charge Transportation of TiO₂ Nanobelts by Deposition of MoS₂ for Enhanced Photocatalytic Removal of Cr(VI). *Catalysts* **2017**, *7*, 30. [[CrossRef](#)]
20. Cai, Z.; Bu, X.; Wang, P.; Ho, J.C.; Yang, J.; Wang, X. Recent advances in layered double hydroxide electrocatalysts for the oxygen evolution reaction. *J. Mater. Chem. A* **2019**, *7*, 5069–5089. [[CrossRef](#)]
21. Yang, D.; Yang, G.; Li, J.; Gai, S.; He, F.; Yang, P. NIR-driven water splitting by layered bismuth oxyhalide sheets for effective photodynamic therapy. *J. Mater. Chem. B* **2017**, *5*, 4152–4161. [[CrossRef](#)] [[PubMed](#)]
22. Qin, J.; Hu, X.; Li, X.; Yin, Z.; Liu, B.; Lam, K.-H. 0D/2D AgInS₂/MXene Z-scheme heterojunction nanosheets for improved ammonia photosynthesis of N₂. *Nano Energy* **2019**, *61*, 27–35. [[CrossRef](#)]
23. Jin, R.; Li, G.; Sharma, S.; Li, Y.; Du, X. Toward Active-Site Tailoring in Heterogeneous Catalysis by Atomically Precise Metal Nanoclusters with Crystallographic Structures. *Chem. Rev.* **2021**, *121*, 567–648. [[CrossRef](#)] [[PubMed](#)]
24. Zheng, W.; Yang, J.; Chen, H.; Hou, Y.; Wang, Q.; Gu, M.; He, F.; Xia, Y.; Xia, Z.; Li, Z.; et al. Atomically Defined Undercoordinated Active Sites for Highly Efficient CO₂ Electroreduction. *Adv. Funct. Mater.* **2020**, *30*, 1907658. [[CrossRef](#)]
25. Raza, A.; Hassan, J.Z.; Ikram, M.; Ali, S.; Farooq, U.; Khan, Q.; Maqbool, M. Advances in Liquid-Phase and Intercalation Exfoliations of Transition Metal Dichalcogenides to Produce 2D Framework. *Adv. Mater. Interfaces* **2021**, *8*, 2002205. [[CrossRef](#)]

26. Kumar, U.; Hassan, J.; Naz, S.; Haider, A.; Raza, A.; Ul-Hamid, A.; Haider, J.; Shahzadi, I.; Ahmad, I.; Ikram, M. Silver decorated 2D nanosheets of GO and MoS₂ serve as nanocatalyst for water treatment and antimicrobial applications as ascertained with molecular docking evaluation. *Nanotechnology* **2021**, *32*, 255704. [[CrossRef](#)]
27. Raza, A.; Hassan, J.Z.; Mahmood, A.; Nabgan, W.; Ikram, M. Recent advances in membrane-enabled water desalination by 2D frameworks: Graphene and beyond. *Desalination* **2022**, *531*, 115684. [[CrossRef](#)]
28. Shi, Q.; Qin, Z.; Waheed, A.; Gao, Y.; Xu, H.; Abroshan, H.; Li, G. Oxygen Vacancy Engineering: An Approach to Promote Photocatalytic Conversion of Methanol to Methyl Formate over CuO/TiO₂-Spindle. *Nano Res.* **2020**, *13*, 939–946. [[CrossRef](#)]
29. Chang, X.; Wang, T.; Yang, P.; Zhang, G.; Gong, J. The Development of Cocatalysts for Photoelectrochemical CO₂ Reduction. *Adv. Mater.* **2019**, *31*, 1804710. [[CrossRef](#)]
30. Zhong, S.; Xi, Y.; Wu, S.; Liu, Q.; Zhao, L.; Bai, S. Hybrid cocatalysts in semiconductor-based photocatalysis and photoelectrocatalysis. *J. Mater. Chem. A* **2020**, *8*, 14863–14894. [[CrossRef](#)]
31. Chen, D.; Liu, Z.; Guo, Z.; Ruan, M.; Yan, W. 3D Branched Ca-Fe₂O₃/Fe₂O₃ Decorated with Pt and Co-Pi: Improved Charge-Separation Dynamics and Photoelectrochemical Performance. *ChemSusChem* **2019**, *12*, 3286–3295. [[CrossRef](#)] [[PubMed](#)]
32. Xu, W.; Tian, W.; Meng, L.; Cao, F.; Li, L. Ion Sputtering-Assisted Double-Side Interfacial Engineering for CdIn₂S₄ Photoanode toward Improved Photoelectrochemical Water Splitting. *Adv. Mater. Interfaces* **2020**, *7*, 1901947. [[CrossRef](#)]
33. Li, H.; Wen, P.; Itanze, D.S.; Kim, M.W.; Adhikari, S.; Lu, C.; Jiang, L.; Qiu, Y.; Geyer, S.M. Phosphorus-Rich Colloidal Cobalt Diphosphide (CoP₂) Nanocrystals for Electrochemical and Photoelectrochemical Hydrogen Evolution. *Adv. Mater.* **2019**, *31*, 1900813. [[CrossRef](#)]
34. Badia-Bou, L.; Mas-Marza, E.; Rodenas, P.; Barea, E.M.; Fabregat-Santiago, F.; Gimenez, S.; Peris, E.; Bisquert, J. Water Oxidation at Hematite Photoelectrodes with an Iridium-Based Catalyst. *J. Phys. Chem. C* **2013**, *117*, 3826–3833. [[CrossRef](#)]
35. Zhong, M.; Hisatomi, T.; Kuang, Y.; Zhao, J.; Liu, M.; Iwase, A.; Jia, Q.; Nishiyama, H.; Minegishi, T.; Nakabayashi, M.; et al. Surface Modification of CoOx Loaded BiVO₄ Photoanodes with Ultrathin p-Type NiO Layers for Improved Solar Water Oxidation. *J. Am. Chem. Soc.* **2015**, *137*, 5053–5060. [[CrossRef](#)] [[PubMed](#)]
36. Kandiel, T.A.; Ahmed, M.G.; Ahmed, A.Y. Physical Insights into Band Bending in Pristine and Co-Pi-Modified BiVO₄ Photoanodes with Dramatically Enhanced Solar Water Splitting Efficiency. *J. Phys. Chem. Lett.* **2020**, *11*, 5015–5020. [[CrossRef](#)] [[PubMed](#)]
37. Wang, Y.; Tian, W.; Cao, F.; Fang, D.; Chen, S.; Li, L. Boosting PEC performance of Si photoelectrodes by coupling bifunctional CuCo hybrid oxide cocatalysts. *Nanotechnology* **2018**, *29*, 425703. [[CrossRef](#)]
38. Wang, Y.; Tian, W.; Chen, C.; Xu, W.; Li, L. Tungsten Trioxide Nanostructures for Photoelectrochemical Water Splitting: Material Engineering and Charge Carrier Dynamic Manipulation. *Adv. Funct. Mater.* **2019**, *29*, 1809036. [[CrossRef](#)]
39. Lei, C.; Lyu, S.; Si, J.; Yang, B.; Li, Z.; Lei, L.; Wen, Z.; Wu, G.; Hou, Y. Nanostructured Carbon Based Heterogeneous Electrocatalysts for Oxygen Evolution Reaction in Alkaline Media. *ChemCatChem* **2019**, *11*, 5855–5874. [[CrossRef](#)]
40. Huang, X.; Zeng, Z.; Fan, Z.; Liu, J.; Zhang, H. Graphene-Based Electrodes. *Adv. Mater.* **2012**, *24*, 5979–6004. [[CrossRef](#)]
41. Guo, S.; Zhang, S.; Fang, Q.; Abroshan, H.; Kim, H.; Haruta, M.; Li, G. Gold-palladium nanoalloys supported by graphene oxide and lamellar TiO₂ for direct synthesis of hydrogen peroxide. *ACS Appl. Mater. Interfaces* **2018**, *10*, 40599–40607. [[CrossRef](#)] [[PubMed](#)]
42. Guo, Y.; Xu, K.; Wu, C.; Zhao, J.; Xie, Y. Surface chemical-modification for engineering the intrinsic physical properties of inorganic two-dimensional nanomaterials. *Chem. Soc. Rev.* **2015**, *44*, 637–646. [[CrossRef](#)] [[PubMed](#)]
43. Zhang, X.; Xie, X.; Wang, H.; Zhang, J.; Pan, B.; Xie, Y. Enhanced Photoresponsive Ultrathin Graphitic-Phase C₃N₄ Nanosheets for Bioimaging. *J. Am. Chem. Soc.* **2013**, *135*, 18–21. [[CrossRef](#)] [[PubMed](#)]
44. Wang, H.; Yang, X.; Shao, W.; Chen, S.; Xie, J.; Zhang, X.; Wang, J.; Xie, Y. Ultrathin Black Phosphorus Nanosheets for Efficient Singlet Oxygen Generation. *J. Am. Chem. Soc.* **2015**, *137*, 11376–11382. [[CrossRef](#)]
45. Zhou, M.; Lou, X.W.; Xie, Y. Two-dimensional nanosheets for photoelectrochemical water splitting: Possibilities and opportunities. *Nano Today* **2013**, *8*, 598–618. [[CrossRef](#)]
46. Sun, Y.; Gao, S.; Lei, F.; Xiao, C.; Xie, Y. Ultrathin Two-Dimensional Inorganic Materials: New Opportunities for Solid State Nanochemistry. *Acc. Chem. Res.* **2015**, *48*, 3–12. [[CrossRef](#)]
47. Yin, Z.; Chen, B.; Bosman, M.; Cao, X.; Chen, J.; Zheng, B.; Zhang, H. Au Nanoparticle-Modified MoS₂ Nanosheet-Based Photoelectrochemical Cells for Water Splitting. *Small* **2014**, *10*, 3537–3543. [[CrossRef](#)]
48. Li, H.; Dong, W.; Zhang, J.; Xi, J.; Du, G.; Ji, Z. MoS₂ nanosheet/ZnO nanowire hybrid nanostructures for photoelectrochemical water splitting. *J. Am. Ceram. Soc.* **2018**, *101*, 3989–3996. [[CrossRef](#)]
49. Masoumi, Z.; Tayebi, M.; Kolaei, M.; Lee, B.-K. Unified surface modification by double heterojunction of MoS₂ nanosheets and BiVO₄ nanoparticles to enhance the photoelectrochemical water splitting of hematite photoanode. *J. Alloys Compd.* **2022**, *890*, 161802. [[CrossRef](#)]
50. Seo, D.-B.; Trung, T.N.; Kim, D.-O.; Duc, D.V.; Hong, S.; Sohn, Y.; Jeong, J.-R.; Kim, E.-T. Plasmonic Ag-Decorated Few-Layer MoS₂ Nanosheets Vertically Grown on Graphene for Efficient Photoelectrochemical Water Splitting. *Nano-Micro Lett.* **2020**, *12*, 172. [[CrossRef](#)]
51. Bhat, S.S.M.; Pawar, S.A.; Potphode, D.; Moon, C.-K.; Suh, J.M.; Kim, C.; Choi, S.; Patil, D.S.; Kim, J.-J.; Shin, J.C.; et al. Substantially enhanced photoelectrochemical performance of TiO₂ nanorods/CdS nanocrystals heterojunction photoanode decorated with MoS₂ nanosheets. *Appl. Catal. B Environ.* **2019**, *259*, 118102. [[CrossRef](#)]

52. Sreedhar, A.; Noh, J.-S. Interfacial engineering insights of promising monolayer 2D Ti_3C_2 MXene anchored flake-like ZnO thin films for improved PEC water splitting. *J. Electroanal. Chem.* **2021**, *883*, 115044. [CrossRef]
53. Yin, H.; Wang, Y.; Ma, L.; Zhang, S.; Yang, B.; Jiang, R. Effect of surface-deposited $\text{Ti}_3\text{C}_2\text{T}_x$ MXene on the photoelectrochemical water-oxidation performance of iron-doped titania nanorod array. *Chem. Eng. J.* **2022**, *431*, 134124. [CrossRef]
54. Ye, R.-K.; Sun, S.-S.; He, L.-Q.; Yang, S.-R.; Liu, X.-Q.; Li, M.-D.; Fang, P.-P.; Hu, J.-Q. Surface engineering of hematite nanorods by 2D Ti_3C_2 -MXene: Suppressing the electron-hole recombination for enhanced photoelectrochemical performance. *Appl. Catal. B Environ.* **2021**, *291*, 120107. [CrossRef]
55. Kumar, D.; Sharma, S.; Khare, N. Enhanced photoelectrochemical performance of NaNbO_3 nanofiber photoanodes coupled with visible light active g- C_3N_4 nanosheets for water splitting. *Nanotechnology* **2020**, *31*, 135402. [CrossRef]
56. Hou, Y.; Wen, Z.; Cui, S.; Feng, X.; Chen, J. Strongly Coupled Ternary Hybrid Aerogels of N-deficient Porous Graphitic- C_3N_4 Nanosheets/N-Doped Graphene/NiFe-Layered Double Hydroxide for Solar-Driven Photoelectrochemical Water Oxidation. *Nano Lett.* **2016**, *16*, 2268–2277. [CrossRef]
57. Babu, B.; Koutavarapu, R.; Shim, J.; Yoo, K. Enhanced visible-light-driven photoelectrochemical and photocatalytic performance of Au- SnO_2 quantum dot-anchored g- C_3N_4 nanosheets. *Sep. Purif. Technol.* **2020**, *240*, 116652. [CrossRef]
58. Arif, M.; Yasin, G.; Shakeel, M.; Fang, X.; Gao, R.; Ji, S.; Yan, D. Coupling of Bifunctional CoMn-Layered Double Hydroxide@Graphitic C_3N_4 Nanohybrids towards Efficient Photoelectrochemical Overall Water Splitting. *Chem. Asian J.* **2018**, *13*, 1045–1052. [CrossRef]
59. Chaudhary, P.; Ingole, P.P. In-Situ solid-state synthesis of 2D/2D interface between Ni/NiO hexagonal nanosheets supported on g- C_3N_4 for enhanced photo-electrochemical water splitting. *Int. J. Hydrogen Energy* **2020**, *45*, 16060–16070. [CrossRef]
60. Basu, M.; Zhang, Z.-W.; Chen, C.-J.; Lu, T.-H.; Hu, S.-F.; Liu, R.-S. CoSe₂ Embedded in C_3N_4 : An Efficient Photocathode for Photoelectrochemical Water Splitting. *ACS Appl. Mater. Interfaces* **2016**, *8*, 26690–26696. [CrossRef]
61. Bai, S.; Chu, H.; Xiang, X.; Luo, R.; He, J.; Chen, A. Fabricating of $\text{Fe}_2\text{O}_3/\text{BiVO}_4$ heterojunction based photoanode modified with NiFe-LDH nanosheets for efficient solar water splitting. *Chem. Eng. J.* **2018**, *350*, 148–156. [CrossRef]
62. Pang, J.; Mendes, R.G.; Bachmatiuk, A.; Zhao, L.; Ta, H.Q.; Gemming, T.; Liu, H.; Liu, Z.; Rummeli, M.H. Applications of 2D MXenes in energy conversion and storage systems. *Chem. Soc. Rev.* **2019**, *48*, 72–133. [CrossRef] [PubMed]
63. Zang, X.; Jian, C.; Zhu, T.; Fan, Z.; Wang, W.; Wei, M.; Li, B.; Follmar Diaz, M.; Ashby, P.; Lu, Z.; et al. Laser-sculptured ultrathin transition metal carbide layers for energy storage and energy harvesting applications. *Nat. Commun.* **2019**, *10*, 3112. [CrossRef]
64. Wang, H.; Sun, Y.; Wu, Y.; Tu, W.; Wu, S.; Yuan, X.; Zeng, G.; Xu, Z.J.; Li, S.; Chew, J.W. Electrical promotion of spatially photoinduced charge separation via interfacial-built-in quasi-alloying effect in hierarchical $\text{Zn}_2\text{In}_2\text{S}_5/\text{Ti}_3\text{C}_2(\text{O}, \text{OH})_x$ hybrids toward efficient photocatalytic hydrogen evolution and environmental remediation. *Appl. Catal. B: Environ.* **2019**, *245*, 290–301. [CrossRef]
65. Peng, J.; Chen, X.; Ong, W.-J.; Zhao, X.; Li, N. Surface and Heterointerface Engineering of 2D MXenes and Their Nanocomposites: Insights into Electro- and Photocatalysis. *Chemistry* **2019**, *5*, 18–50. [CrossRef]
66. Song, Y.; Zhang, X.; Zhang, Y.; Zhai, P.; Li, Z.; Jin, D.; Cao, J.; Wang, C.; Zhang, B.; Gao, J.; et al. Engineering MoOx/MXene Hole Transfer Layers for Unexpected Boosting Photoelectrochemical Water Oxidation. *Angew. Chem. Int. Ed.* **2022**, *n/a*, e202200946. [CrossRef]
67. Li, Z.; Wang, P.; Ma, C.; Igbari, F.; Kang, Y.; Wang, K.-L.; Song, W.; Dong, C.; Li, Y.; Yao, J.; et al. Single-Layered MXene Nanosheets Doping TiO_2 for Efficient and Stable Double Perovskite Solar Cells. *J. Am. Chem. Soc.* **2021**, *143*, 2593–2600. [CrossRef]
68. Le, T.A.; Bui, Q.V.; Tran, N.Q.; Cho, Y.; Hong, Y.; Kawazoe, Y.; Lee, H. Synergistic Effects of Nitrogen Doping on MXene for Enhancement of Hydrogen Evolution Reaction. *ACS Sustain. Chem. Eng.* **2019**, *7*, 16879–16888. [CrossRef]
69. Zhang, Y.; Jiang, H.; Lin, Y.; Liu, H.; He, Q.; Wu, C.; Duan, T.; Song, L. In Situ Growth of Cobalt Nanoparticles Encapsulated Nitrogen-Doped Carbon Nanotubes among $\text{Ti}_3\text{C}_2\text{T}_x$ (MXene) Matrix for Oxygen Reduction and Evolution. *Adv. Mater. Interfaces* **2018**, *5*, 1800392. [CrossRef]
70. Zhou, S.; Yang, X.; Pei, W.; Liu, N.; Zhao, J. Heterostructures of MXenes and N-doped graphene as highly active bifunctional electrocatalysts. *Nanoscale* **2018**, *10*, 10876–10883. [CrossRef]
71. Habib, T.; Zhao, X.; Shah, S.A.; Chen, Y.; Sun, W.; An, H.; Lutkenhaus, J.L.; Radovic, M.; Green, M.J. Oxidation stability of $\text{Ti}_3\text{C}_2\text{T}_x$ MXene nanosheets in solvents and composite films. *npj 2D Mater. Appl.* **2019**, *3*, 8. [CrossRef]
72. Anasori, B.; Lukatskaya, M.R.; Gogotsi, Y. 2D metal carbides and nitrides (MXenes) for energy storage. *Nat. Rev. Mater.* **2017**, *2*, 16098. [CrossRef]
73. Bhat, A.; Anwer, S.; Bhat, K.S.; Mohideen, M.I.H.; Liao, K.; Qurashi, A. Prospects challenges and stability of 2D MXenes for clean energy conversion and storage applications. *npj 2D Mater. Appl.* **2021**, *5*, 61. [CrossRef]
74. Daulbayev, C.; Sultanov, F.; Bakbolat, B.; Daulbayev, O. 0D, 1D and 2D nanomaterials for visible photoelectrochemical water splitting. A Review. *Int. J. Hydrogen Energy* **2020**, *45*, 33325–33342. [CrossRef]
75. Wu, X.; Wang, Z.; Yu, M.; Xiu, L.; Qiu, J. Stabilizing the MXenes by Carbon Nanopating for Developing Hierarchical Nanohybrids with Efficient Lithium Storage and Hydrogen Evolution Capability. *Adv. Mater.* **2017**, *29*, 1607017. [CrossRef]
76. Chen, J.; Yuan, X.; Lyu, F.; Zhong, Q.; Hu, H.; Pan, Q.; Zhang, Q. Integrating MXene nanosheets with cobalt-tipped carbon nanotubes for an efficient oxygen reduction reaction. *J. Mater. Chem. A* **2019**, *7*, 1281–1286. [CrossRef]

77. Quan, Q.; Zhang, T.; Lei, C.; Yang, B.; Li, Z.; Chen, J.; Yuan, C.; Lei, L.; Hou, Y. Confined carburization-engineered synthesis of ultrathin nickel oxide/nickel heterostructured nanosheets for enhanced oxygen evolution reaction. *Nanoscale* **2019**, *11*, 22261–22269. [[CrossRef](#)]
78. Li, Y.; Li, Y.-L.; Araujo, C.M.; Luo, W.; Ahuja, R. Single-layer MoS₂ as an efficient photocatalyst. *Catal. Sci. Technol.* **2013**, *3*, 2214–2220. [[CrossRef](#)]
79. Chen, Z.; Forman, A.J.; Jaramillo, T.F. Bridging the Gap Between Bulk and Nanostructured Photoelectrodes: The Impact of Surface States on the Electrocatalytic and Photoelectrochemical Properties of MoS₂. *J. Phys. Chem. C* **2013**, *117*, 9713–9722. [[CrossRef](#)]
80. Chang, K.; Mei, Z.; Wang, T.; Kang, Q.; Ouyang, S.; Ye, J. MoS₂/Graphene Cocatalyst for Efficient Photocatalytic H₂ Evolution under Visible Light Irradiation. *ACS Nano* **2014**, *8*, 7078–7087. [[CrossRef](#)]
81. Guo, C.; Tong, X.; Guo, X.-Y. Solvothermal synthesis of FeS₂ nanoparticles for photoelectrochemical hydrogen generation in neutral water. *Mater. Lett.* **2015**, *161*, 220–223. [[CrossRef](#)]
82. Liu, Y.; Cheng, H.; Lyu, M.; Fan, S.; Liu, Q.; Zhang, W.; Zhi, Y.; Wang, C.; Xiao, C.; Wei, S.; et al. Low Overpotential in Vacancy-Rich Ultrathin CoSe₂ Nanosheets for Water Oxidation. *J. Am. Chem. Soc.* **2014**, *136*, 15670–15675. [[CrossRef](#)]
83. Kwak, I.H.; Im, H.S.; Jang, D.M.; Kim, Y.W.; Park, K.; Lim, Y.R.; Cha, E.H.; Park, J. CoSe₂ and NiSe₂ Nanocrystals as Superior Bifunctional Catalysts for Electrochemical and Photoelectrochemical Water Splitting. *ACS Appl. Mater. Interfaces* **2016**, *8*, 5327–5334. [[CrossRef](#)] [[PubMed](#)]
84. Wang, L.; Cao, J.; Lei, C.; Dai, Q.; Yang, B.; Li, Z.; Zhang, X.; Yuan, C.; Lei, L.; Hou, Y. Strongly Coupled 3D N-Doped MoO₂/Ni₃S₂ Hybrid for High Current Density Hydrogen Evolution Electrocatalysis and Biomass Upgrading. *ACS Appl. Mater. Interfaces* **2019**, *11*, 27743–27750. [[CrossRef](#)] [[PubMed](#)]
85. Hou, Y.; Qiu, M.; Nam, G.; Kim, M.G.; Zhang, T.; Liu, K.; Zhuang, X.; Cho, J.; Yuan, C.; Feng, X. Integrated Hierarchical Cobalt Sulfide/Nickel Selenide Hybrid Nanosheets as an Efficient Three-dimensional Electrode for Electrochemical and Photoelectrochemical Water Splitting. *Nano Lett.* **2017**, *17*, 4202–4209. [[CrossRef](#)]
86. Li, Y.; Shi, J.; Mi, Y.; Sui, X.; Xu, H.; Liu, X. Ultrafast carrier dynamics in two-dimensional transition metal dichalcogenides. *J. Mater. Chem. C* **2019**, *7*, 4304–4319. [[CrossRef](#)]
87. Ke, J.; Liu, J.; Sun, H.; Zhang, H.; Duan, X.; Liang, P.; Li, X.; Tade, M.O.; Liu, S.; Wang, S. Facile assembly of Bi₂O₃/Bi₂S₃/MoS₂ n-p heterojunction with layered n-Bi₂O₃ and p-MoS₂ for enhanced photocatalytic water oxidation and pollutant degradation. *Appl. Catal. B Environ.* **2017**, *200*, 47–55. [[CrossRef](#)]
88. Rosman, N.N.; Mohamad Yunus, R.; Jeffery Minggu, L.; Arifin, K.; Salehmin, M.N.I.; Mohamed, M.A.; Kassim, M.B. Photocatalytic properties of two-dimensional graphene and layered transition-metal dichalcogenides based photocatalyst for photoelectrochemical hydrogen generation: An overview. *Int. J. Hydrogen Energy* **2018**, *43*, 18925–18945. [[CrossRef](#)]
89. Carraro, F.; Calvillo, L.; Cattelan, M.; Favaro, M.; Righetto, M.; Nappini, S.; Piš, I.; Celorrio, V.; Fermín, D.J.; Martucci, A.; et al. Fast One-Pot Synthesis of MoS₂/Crumpled Graphene p–n Nanonjunctions for Enhanced Photoelectrochemical Hydrogen Production. *ACS Appl. Mater. Interfaces* **2015**, *7*, 25685–25692. [[CrossRef](#)]
90. Ranjan, R.; Kumar, M.; Sinha, A.S.K. Development and characterization of rGO supported CdSMoS₂ photoelectrochemical catalyst for splitting water by visible light. *Int. J. Hydrogen Energy* **2019**, *44*, 16176–16189. [[CrossRef](#)]
91. Jiao, Y.; Huang, Q.; Wang, J.; He, Z.; Li, Z. A novel MoS₂ quantum dots (QDs) decorated Z-scheme g-C₃N₄ nanosheet/N-doped carbon dots heterostructure photocatalyst for photocatalytic hydrogen evolution. *Appl. Catal. B Environ.* **2019**, *247*, 124–132. [[CrossRef](#)]
92. Li, N.; Liu, Z.; Liu, M.; Xue, C.; Chang, Q.; Wang, H.; Li, Y.; Song, Z.; Hu, S. Facile Synthesis of Carbon Dots@2D MoS₂ Heterostructure with Enhanced Photocatalytic Properties. *Inorg. Chem.* **2019**, *58*, 5746–5752. [[CrossRef](#)] [[PubMed](#)]
93. Zheng, J.; Zhang, R.; Wang, X.; Yu, P. Importance of carbon quantum dots for improving the electrochemical performance of MoS₂@ZnS composite. *J. Mater. Sci.* **2019**, *54*, 13509–13522. [[CrossRef](#)]
94. Zhao, S.; Li, C.; Wang, L.; Liu, N.; Qiao, S.; Liu, B.; Huang, H.; Liu, Y.; Kang, Z. Carbon quantum dots modified MoS₂ with visible-light-induced high hydrogen evolution catalytic ability. *Carbon* **2016**, *99*, 599–606. [[CrossRef](#)]
95. Liu, Y.; Zhang, H.; Ke, J.; Zhang, J.; Tian, W.; Xu, X.; Duan, X.; Sun, H.; O Tade, M.; Wang, S. 0D (MoS₂)/2D (g-C₃N₄) heterojunctions in Z-scheme for enhanced photocatalytic and electrochemical hydrogen evolution. *Appl. Catal. B Environ.* **2018**, *228*, 64–74. [[CrossRef](#)]
96. Zhang, X.; Yang, Y.; Huang, W.; Yang, Y.; Wang, Y.; He, C.; Liu, N.; Wu, M.; Tang, L. g-C₃N₄/UiO-66 nanohybrids with enhanced photocatalytic activities for the oxidation of dye under visible light irradiation. *Mater. Res. Bull.* **2018**, *99*, 349–358. [[CrossRef](#)]
97. Raza, A.; Altaf, S.; Ali, S.; Ikram, M.; Li, G. Recent Advances in Carbonaceous Sustainable Nanomaterials for Wastewater Treatments. *Sustain. Mater. Technol.* **2022**, *32*, e00406. [[CrossRef](#)]
98. Liu, Q.; Chen, T.; Guo, Y.; Zhang, Z.; Fang, X. Ultrathin g-C₃N₄ nanosheets coupled with carbon nanodots as 2D/0D composites for efficient photocatalytic H₂ evolution. *Appl. Catal. B Environ.* **2016**, *193*, 248–258. [[CrossRef](#)]
99. Faraji, M.; Yousefi, M.; Yousefzadeh, S.; Zirak, M.; Naseri, N.; Jeon, T.H.; Choi, W.; Moshfegh, A.Z. Two-dimensional materials in semiconductor photoelectrocatalytic systems for water splitting. *Energy Environ. Sci.* **2019**, *12*, 59–95. [[CrossRef](#)]
100. Gao, G.; Jiao, Y.; Ma, F.; Jiao, Y.; Waclawik, E.; Du, A. Carbon nanodot decorated graphitic carbon nitride: New insights into the enhanced photocatalytic water splitting from ab initio studies. *Phys. Chem. Chem. Phys.* **2015**, *17*, 31140–31144. [[CrossRef](#)]
101. Liu, J.; Liu, Y.; Liu, N.; Han, Y.; Zhang, X.; Huang, H.; Lifshitz, Y.; Lee, S.-T.; Zhong, J.; Kang, Z. Metal-free efficient photocatalyst for stable visible water splitting via a two-electron pathway. *Science* **2015**, *347*, 970. [[CrossRef](#)] [[PubMed](#)]

102. Wei, Y.; Wang, Z.; Su, J.; Guo, L. Metal-Free Flexible Protonated g-C₃N₄/Carbon Dots Photoanode for Photoelectrochemical Water Splitting. *ChemElectroChem* **2018**, *5*, 2734–2737. [[CrossRef](#)]
103. Peng, G.; Volokh, M.; Tzadikov, J.; Sun, J.; Shalom, M. Carbon Nitride/Reduced Graphene Oxide Film with Enhanced Electron Diffusion Length: An Efficient Photo-Electrochemical Cell for Hydrogen Generation. *Adv. Energy Mater.* **2018**, *8*, 1800566. [[CrossRef](#)]
104. Hou, Y.; Wen, Z.; Cui, S.; Guo, X.; Chen, J. Constructing 2D Porous Graphitic C₃N₄ Nanosheets/Nitrogen-Doped Graphene/Layered MoS₂ Ternary Nanojunction with Enhanced Photoelectrochemical Activity. *Adv. Mater.* **2013**, *25*, 6291–6297. [[CrossRef](#)]
105. Gao, X.; Zhu, Y.; Yi, D.; Zhou, J.; Zhang, S.; Yin, C.; Ding, F.; Zhang, S.; Yi, X.; Wang, J.; et al. Ultrathin graphdiyne film on graphene through solution-phase van der Waals epitaxy. *Sci. Adv.* **2018**, *4*, eaat6378. [[CrossRef](#)]
106. Gao, X.; Li, J.; Du, R.; Zhou, J.; Huang, M.-Y.; Liu, R.; Li, J.; Xie, Z.; Wu, L.-Z.; Liu, Z.; et al. Direct Synthesis of Graphdiyne Nanowalls on Arbitrary Substrates and Its Application for Photoelectrochemical Water Splitting Cell. *Adv. Mater.* **2017**, *29*, 1605308. [[CrossRef](#)]
107. Li, J.; Gao, X.; Liu, B.; Feng, Q.; Li, X.-B.; Huang, M.-Y.; Liu, Z.; Zhang, J.; Tung, C.-H.; Wu, L.-Z. Graphdiyne: A Metal-Free Material as Hole Transfer Layer To Fabricate Quantum Dot-Sensitized Photocathodes for Hydrogen Production. *J. Am. Chem. Soc.* **2016**, *138*, 3954–3957. [[CrossRef](#)]
108. Han, Y.-Y.; Lu, X.-L.; Tang, S.-F.; Yin, X.-P.; Wei, Z.-W.; Lu, T.-B. Metal-Free 2D/2D Heterojunction of Graphitic Carbon Nitride/Graphdiyne for Improving the Hole Mobility of Graphitic Carbon Nitride. *Adv. Energy Mater.* **2018**, *8*, 1702992. [[CrossRef](#)]
109. Gao, R.; Yan, D. Recent Development of Ni/Fe-Based Micro/Nanostructures toward Photo/Electrochemical Water Oxidation. *Adv. Energy Mater.* **2019**, *10*, 1900954. [[CrossRef](#)]
110. Mohammed-Ibrahim, J. A review on NiFe-based electrocatalysts for efficient alkaline oxygen evolution reaction. *J. Power Sources* **2020**, *448*, 227375. [[CrossRef](#)]
111. Zhang, W.; Li, D.; Zhang, L.; She, X.; Yang, D. NiFe-based nanostructures on nickel foam as highly efficiently electrocatalysts for oxygen and hydrogen evolution reactions. *J. Energy Chem.* **2019**, *39*, 39–53. [[CrossRef](#)]
112. Kment, S.; Riboni, F.; Pausova, S.; Wang, L.; Wang, L.; Han, H.; Hubicka, Z.; Krysa, J.; Schmuki, P.; Zboril, R. Photoanodes based on TiO₂ and α-Fe₂O₃ for solar water splitting—Superior role of 1D nanoarchitectures and of combined heterostructures. *Chem. Soc. Rev.* **2017**, *46*, 3716–3769. [[CrossRef](#)] [[PubMed](#)]
113. Cao, Y.; Guo, S.; Yu, C.; Zhang, J.; Pan, X.; Li, G. Ionic liquid-assisted one-step preparation of ultrafine amorphous metallic hydroxide nanoparticles for the highly efficient oxygen evolution reaction. *J. Mater. Chem. A* **2020**, *8*, 15767–15773. [[CrossRef](#)]
114. Ke, J.; Zhou, H.; Liu, J.; Duan, X.; Zhang, H.; Liu, S.; Wang, S. Crystal transformation of 2D tungstic acid H₂WO₄ to WO₃ for enhanced photocatalytic water oxidation. *J. Colloid Interface Sci.* **2018**, *514*, 576–583. [[CrossRef](#)] [[PubMed](#)]
115. Gao, X.; Lv, H.; Li, Z.; Xu, Q.; Liu, H.; Wang, Y.; Xia, Y. Low-cost and high-performance of a vertically grown 3D Ni–Fe layered double hydroxide/graphene aerogel supercapacitor electrode material. *RSC Adv.* **2016**, *6*, 107278–107285. [[CrossRef](#)]
116. Huang, J.; Hu, G.; Ding, Y.; Pang, M.; Ma, B. Mn-doping and NiFe layered double hydroxide coating: Effective approaches to enhancing the performance of α-Fe₂O₃ in photoelectrochemical water oxidation. *J. Catal.* **2016**, *340*, 261–269. [[CrossRef](#)]
117. Zhang, R.; Shao, M.; Xu, S.; Ning, F.; Zhou, L.; Wei, M. Photo-assisted synthesis of zinc-iron layered double hydroxides/TiO₂ nanoarrays toward highly-efficient photoelectrochemical water splitting. *Nano Energy* **2017**, *33*, 21–28. [[CrossRef](#)]
118. Ganiyu, S.O.; Huong Le, T.X.; Bechelany, M.; Esposito, G.; van Hullebusch, E.D.; Oturan, M.A.; Cretin, M. A hierarchical CoFe-layered double hydroxide modified carbon-felt cathode for heterogeneous electro-Fenton process. *J. Mater. Chem. A* **2017**, *5*, 3655–3666. [[CrossRef](#)]
119. Tang, Y.; Wang, R.; Yang, Y.; Yan, D.; Xiang, X. Highly Enhanced Photoelectrochemical Water Oxidation Efficiency Based on Triadic Quantum Dot/Layered Double Hydroxide/BiVO₄ Photoanodes. *ACS Appl. Mater. Interfaces* **2016**, *8*, 19446–19455. [[CrossRef](#)]
120. Zhao, Y.; Li, B.; Wang, Q.; Gao, W.; Wang, C.J.; Wei, M.; Evans, D.G.; Duan, X.; O’Hare, D. NiTi-Layered double hydroxides nanosheets as efficient photocatalysts for oxygen evolution from water using visible light. *Chem. Sci.* **2014**, *5*, 951–958. [[CrossRef](#)]
121. Boppella, R.; Choi, C.H.; Moon, J.; Ha Kim, D. Spatial charge separation on strongly coupled 2D-hybrid of rGO/La₂Ti₂O₇/NiFe-LDH heterostructures for highly efficient noble metal free photocatalytic hydrogen generation. *Appl. Catal. B Environ.* **2018**, *239*, 178–186. [[CrossRef](#)]
122. Mohapatra, L.; Parida, K. A review on the recent progress, challenges and perspective of layered double hydroxides as promising photocatalysts. *J. Mater. Chem. A* **2016**, *4*, 10744–10766. [[CrossRef](#)]
123. Shao, M.; Ning, F.; Wei, M.; Evans, D.G.; Duan, X. Hierarchical Nanowire Arrays Based on ZnO Core–Layered Double Hydroxide Shell for Largely Enhanced Photoelectrochemical Water Splitting. *Adv. Funct. Mater.* **2013**, *24*, 580–586. [[CrossRef](#)]
124. Wang, Q.; O’Hare, D. Recent advances in the synthesis and application of layered double hydroxide (LDH) nanosheets. *Chem. Rev.* **2012**, *112*, 4124–4155. [[CrossRef](#)] [[PubMed](#)]
125. Ren, L.; Wang, C.; Li, W.; Dong, R.; Sun, H.; Liu, N.; Geng, B. Heterostructural NiFe-LDH@Ni₃S₂ nanosheet arrays as an efficient electrocatalyst for overall water splitting. *Electrochim. Acta* **2019**, *318*, 42–50. [[CrossRef](#)]
126. Liu, P.F.; Yang, S.; Zhang, B.; Yang, H.G. Defect-Rich Ultrathin Cobalt-Iron Layered Double Hydroxide for Electrochemical Overall Water Splitting. *ACS Appl. Mater. Interfaces* **2016**, *8*, 34474–34481. [[CrossRef](#)]
127. Liu, X.; Wu, Y.; Xie, G.; Wang, Z.; Li, Y.; Li, Q. New Green Soft Chemistry Route to Ag-Cu Bimetallic Nanomaterials. *Int. J. Electrochem. Sci.* **2017**, *12*, 3275–3282. [[CrossRef](#)]

128. Chen, H.; Zhao, Q.; Gao, L.; Ran, J.; Hou, Y. Water-Plasma Assisted Synthesis of Oxygen-Enriched Ni-Fe Layered Double Hydroxide Nanosheets for Efficient Oxygen Evolution Reaction. *ACS Sustain. Chem. Eng.* **2019**, *7*, 4247–4254. [[CrossRef](#)]
129. Lv, L.; Yang, Z.; Chen, K.; Wang, C.; Xiong, Y. 2D Layered Double Hydroxides for Oxygen Evolution Reaction: From Fundamental Design to Application. *Adv. Energy Mater.* **2019**, *9*, 1803358. [[CrossRef](#)]
130. Gong, M.; Li, Y.; Wang, H.; Liang, Y.; Wu, J.Z.; Zhou, J.; Wang, J.; Regier, T.; Wei, F.; Dai, H. An advanced Ni-Fe layered double hydroxide electrocatalyst for water oxidation. *J. Am. Chem. Soc.* **2013**, *135*, 8452–8455. [[CrossRef](#)]
131. Tang, D.; Han, Y.; Ji, W.; Qiao, S.; Zhou, X.; Liu, R.; Han, X.; Huang, H.; Liu, Y.; Kang, Z. A high-performance reduced graphene oxide/ZnCo layered double hydroxide electrocatalyst for efficient water oxidation. *Dalton Trans.* **2014**, *43*, 15119–15125. [[CrossRef](#)] [[PubMed](#)]
132. Youn, D.H.; Park, Y.B.; Kim, J.Y.; Magesh, G.; Jang, Y.J.; Lee, J.S. One-pot synthesis of NiFe layered double hydroxide/reduced graphene oxide composite as an efficient electrocatalyst for electrochemical and photoelectrochemical water oxidation. *J. Power Sources* **2015**, *294*, 437–443. [[CrossRef](#)]
133. Li, J.; Gao, X.; Li, Z.; Wang, J.H.; Zhu, L.; Yin, C.; Wang, Y.; Li, X.B.; Liu, Z.; Zhang, J.; et al. Superhydrophilic Graphdiyne Accelerates Interfacial Mass/Electron Transportation to Boost Electrocatalytic and Photoelectrocatalytic Water Oxidation Activity. *Adv. Funct. Mater.* **2019**, *29*, 1808079. [[CrossRef](#)]
134. Sun, L.; Sun, J.; Yang, X.; Bai, S.; Feng, Y.; Luo, R.; Li, D.; Chen, A. An integrating photoanode consisting of BiVO₄, rGO and LDH for photoelectrochemical water splitting. *Dalton Trans.* **2019**, *48*, 16091–16098. [[CrossRef](#)]
135. Waheed, A.; Shi, Q.; Maeda, N.; Meier, D.M.; Qin, Z.; Li, G.; Baiker, A. Strong Activity Enhancement of the Photocatalytic Degradation of an Azo Dye on Au/TiO₂ Doped with FeO_x. *Catalysts* **2020**, *10*, 933. [[CrossRef](#)]
136. Zhang, S.; Gong, X.; Shi, Q.; Ping, G.; Xu, H.; Waleed, A.; Li, G. CuO Nanoparticle-Decorated TiO₂-Nanotube Heterojunctions for Direct Synthesis of Methyl Formate via Photo-Oxidation of Methanol. *ACS Omega* **2020**, *5*, 15942–15948. [[CrossRef](#)]
137. Liu, J.; Ke, J.; Li, Y.; Liu, B.; Wang, L.; Xiao, H.; Wang, S. Co₃O₄ quantum dots/TiO₂ nanobelt hybrids for highly efficient photocatalytic overall water splitting. *Appl. Catal. B Environ.* **2018**, *236*, 396–403. [[CrossRef](#)]
138. Shi, Q.; Ping, G.; Wang, X.; Xu, H.; Li, J.; Cui, J.; Abroshan, H.; Ding, H.; Li, G. CuO/TiO₂ Heterojunction Composite: An Efficient Photocatalyst for Selective Oxidation of Methanol to Methyl Formate. *J. Mater. Chem. A* **2019**, *7*, 2253–2260. [[CrossRef](#)]
139. Ikram, M.; Raza, A.; Ali, S.; Ali, S. *Electrochemical Exfoliation of 2D Advanced Carbon Derivatives*; IntechOpen: London, UK, 2020. [[CrossRef](#)]
140. Shi, Q.; Wei, X.; Raza, A.; Li, G. Recent Advances in Aerobic Photo-Oxidation of Methanol to Valuable Chemicals. *ChemCatChem* **2021**, *13*, 3381–3395. [[CrossRef](#)]
141. Ikram, M.; Rashid, M.; Haider, A.; Naz, S.; Haider, J.; Raza, A.; Ansar, M.T.; Uddin, M.K.; Ali, N.M.; Ahmed, S.S.; et al. A review of photocatalytic characterization, and environmental cleaning, of metal oxide nanostructured materials. *Sustain. Mater. Technol.* **2021**, *30*, e00343. [[CrossRef](#)]
142. Ning, F.; Shao, M.; Xu, S.; Fu, Y.; Zhang, R.; Wei, M.; Evans, D.G.; Duan, X. TiO₂/graphene/NiFe-layered double hydroxide nanorod array photoanodes for efficient photoelectrochemical water splitting. *Energy Environ. Sci.* **2016**, *9*, 2633–2643. [[CrossRef](#)]
143. Zhang, X.; Wang, R.; Li, F.; An, Z.; Pu, M.; Xiang, X. Enhancing Photoelectrochemical Water Oxidation Efficiency of BiVO₄ Photoanodes by a Hybrid Structure of Layered Double Hydroxide and Graphene. *Ind. Eng. Chem. Res.* **2017**, *56*, 10711–10719. [[CrossRef](#)]
144. Lv, X.; Xiao, X.; Cao, M.; Bu, Y.; Wang, C.; Wang, M.; Shen, Y. Efficient carbon dots/NiFe-layered double hydroxide/BiVO₄ photoanodes for photoelectrochemical water splitting. *Appl. Surf. Sci.* **2018**, *439*, 1065–1071. [[CrossRef](#)]
145. Yu, X.; Prévot, M.S.; Sivula, K. Multiflake Thin Film Electronic Devices of Solution Processed 2D MoS₂ Enabled by Sonopolymer Assisted Exfoliation and Surface Modification. *Chem. Mater.* **2014**, *26*, 5892–5899. [[CrossRef](#)]
146. Yu, X.; Rahmanudin, A.; Jeanbourquin, X.A.; Tsokkou, D.; Guijarro, N.; Banerji, N.; Sivula, K. Hybrid Heterojunctions of Solution-Processed Semiconducting 2D Transition Metal Dichalcogenides. *ACS Energy Lett.* **2017**, *2*, 524–531. [[CrossRef](#)]
147. Pesci, F.M.; Sokolikova, M.S.; Grotta, C.; Sherrell, P.C.; Reale, F.; Sharda, K.; Ni, N.; Palczynski, P.; Mattevi, C. MoS₂/WS₂ Heterojunction for Photoelectrochemical Water Oxidation. *ACS Catal.* **2017**, *7*, 4990–4998. [[CrossRef](#)]
148. Lee, C.-H.; Lee, G.-H.; van der Zande, A.M.; Chen, W.; Li, Y.; Han, M.; Cui, X.; Arefe, G.; Nuckolls, C.; Heinz, T.F.; et al. Atomically thin p-n junctions with van der Waals heterointerfaces. *Nat. Nanotechnol.* **2014**, *9*, 676–681. [[CrossRef](#)]
149. Rigosi, A.F.; Hill, H.M.; Li, Y.; Chernikov, A.; Heinz, T.F. Probing Interlayer Interactions in Transition Metal Dichalcogenide Heterostructures by Optical Spectroscopy: MoS₂/WS₂ and MoSe₂/WSe₂. *Nano Lett.* **2015**, *15*, 5033–5038. [[CrossRef](#)]
150. Palummo, M.; Bernardi, M.; Grossman, J.C. Exciton Radiative Lifetimes in Two-Dimensional Transition Metal Dichalcogenides. *Nano Lett.* **2015**, *15*, 2794–2800. [[CrossRef](#)]
151. Yang, M.-Q.; Xu, Y.-J.; Lu, W.; Zeng, K.; Zhu, H.; Xu, Q.-H.; Ho, G.W. Self-surface charge exfoliation and electrostatically coordinated 2D hetero-layered hybrids. *Nat. Commun.* **2017**, *8*, 14224. [[CrossRef](#)]
152. Zhang, H.; Ji, J.; Gonzalez, A.A.; Choi, J.H. Tailoring photoelectrochemical properties of semiconducting transition metal dichalcogenide nanolayers with porphyrin functionalization. *J. Mater. Chem. C* **2017**, *5*, 11233–11238. [[CrossRef](#)]
153. Choi, J.; Zhang, H.; Choi, J.H. Modulating Optoelectronic Properties of Two-Dimensional Transition Metal Dichalcogenide Semiconductors by Photoinduced Charge Transfer. *ACS Nano* **2016**, *10*, 1671–1680. [[CrossRef](#)] [[PubMed](#)]

154. Zhang, H.; Choi, J.; Ramani, A.; Voiry, D.; Natoli, S.N.; Chhowalla, M.; McMillin, D.R.; Choi, J.H. Engineering Chemically Exfoliated Large-Area Two-Dimensional MoS₂ Nanolayers with Porphyrins for Improved Light Harvesting. *ChemPhysChem* **2016**, *17*, 2854–2862. [[CrossRef](#)]
155. Yan, J.; Chen, Z.; Ji, H.; Liu, Z.; Wang, X.; Xu, Y.; She, X.; Huang, L.; Xu, L.; Xu, H.; et al. Construction of a 2D Graphene-Like MoS₂/C₃N₄ Heterojunction with Enhanced Visible-Light Photocatalytic Activity and Photoelectrochemical Activity. *Chem. Eur. J.* **2016**, *22*, 4764–4773. [[CrossRef](#)] [[PubMed](#)]
156. Biroju, R.K.; Das, D.; Sharma, R.; Pal, S.; Mawlong, L.P.L.; Bhorkar, K.; Giri, P.K.; Singh, A.K.; Narayanan, T.N. Hydrogen Evolution Reaction Activity of Graphene–MoS₂ van der Waals Heterostructures. *ACS Energy Lett.* **2017**, *2*, 1355–1361. [[CrossRef](#)]
157. Lee, H.J.; Lee, B.J.; Kang, D.; Jang, Y.J.; Lee, J.S.; Shin, H.S. 2D materials-based photoelectrochemical cells: Combination of transition metal dichalcogenides and reduced graphene oxide for efficient charge transfer. *FlatChem* **2017**, *4*, 54–60. [[CrossRef](#)]
158. Zhu, M.; Zhai, C.; Fujitsuka, M.; Majima, T. Noble metal-free near-infrared-driven photocatalyst for hydrogen production based on 2D hybrid of black Phosphorus/WS₂. *Appl. Catal. B Environ.* **2018**, *221*, 645–651. [[CrossRef](#)]
159. Delacou, C.; Jeon, I.; Otsuka, K.; Inoue, T.; Anisimov, A.; Fujii, T.; Kauppinen, E.I.; Maruyama, S.; Matsuo, Y. Investigation of charge interaction between fullerene derivatives and single-walled carbon nanotubes. *InfoMat* **2019**, *1*, 559–570. [[CrossRef](#)]
160. Liu, C.; Liu, F.; Li, H.; Chen, J.; Fei, J.; Yu, Z.; Yuan, Z.; Wang, C.; Zheng, H.; Liu, Z.; et al. One-Dimensional van der Waals Heterostructures as Efficient Metal-Free Oxygen Electrocatalysts. *ACS Nano* **2021**, *15*, 3309–3319. [[CrossRef](#)]
161. Jiang, X.; Jang, H.; Liu, S.; Li, Z.; Kim, M.G.; Li, C.; Qin, Q.; Liu, X.; Cho, J. The Heterostructure of Ru₂P/WO₃/NPC Synergistically Promotes H₂O Dissociation for Improved Hydrogen Evolution. *Angew. Chem. Int. Ed.* **2021**, *60*, 4110–4116. [[CrossRef](#)]
162. Yuan, Z.; Li, J.; Yang, M.; Fang, Z.; Jian, J.; Yu, D.; Chen, X.; Dai, L. Ultrathin Black Phosphorus-on-Nitrogen Doped Graphene for Efficient Overall Water Splitting: Dual Modulation Roles of Directional Interfacial Charge Transfer. *J. Am. Chem. Soc.* **2019**, *141*, 4972–4979. [[CrossRef](#)] [[PubMed](#)]
163. Zhang, Z.; Wang, H.; Li, Y.; Xie, M.; Li, C.; Lu, H.; Peng, Y.; Shi, Z. Confined Pyrolysis Synthesis of Well-dispersed Cobalt Copper Bimetallic Three-dimensional N-Doped Carbon Framework as Efficient Water Splitting Electrocatalyst. *Chem. Res. Chin. Univ.* **2022**. [[CrossRef](#)]
164. Zhang, X.; Li, Z.; Pei, W.; Li, G.; Liu, W.; Du, P.; Wang, Z.; Qin, Z.; Qi, H.; Liu, X.; et al. Crystal Phase Mediated Restructuring of Pt on TiO₂ with Tunable Reactivity: Redispersion versus Reshaping. *ACS Catal.* **2022**, *12*, 3634–3643. [[CrossRef](#)]
165. Wang, X.; Zheng, Y.; Sheng, W.; Xu, Z.J.; Jaroniec, M.; Qiao, S.-Z. Strategies for design of electrocatalysts for hydrogen evolution under alkaline conditions. *Mater. Today* **2020**, *36*, 125–138. [[CrossRef](#)]
166. Qin, Z.; Hu, S.; Han, W.; Li, Z.; Xu, W.W.; Zhang, J.; Li, G. Tailoring optical and photocatalytic properties by single-Ag-atom exchange in Au₁₃Ag₁₂(PPh₃)₁₀C₁₈ nanoclusters. *Nano Res.* **2022**, *15*. [[CrossRef](#)]
167. Chen, Q.; Qin, Z.; Liu, S.; Zhu, M.; Li, G. On the Redox Property of Ag₁₆Au₁₃ Clusters and Its Catalytic Application in the Photooxidation. *J. Chem. Phys.* **2021**, *154*, 164308. [[CrossRef](#)]
168. Shi, Q.; Qin, Z.; Sharma, S.; Li, G. Recent progress in heterogeneous catalysis over atomically and structurally precise metal nanoclusters. *Chem. Rec.* **2021**, *21*, 879–892. [[CrossRef](#)]
169. Qin, Z.; Sharma, S.; Wan, C.-Q.; Malola, S.; Xu, W.-w.; Häkkinen, H.; Li, G. A Homoleptic Alkynyl-Ligated [Au₁₃Ag₁₆L₂₄]₃-Cluster as a Catalytically Active Eight-Electron Superatom. *Angew. Chem. Int. Ed.* **2020**, *59*, 970–975.